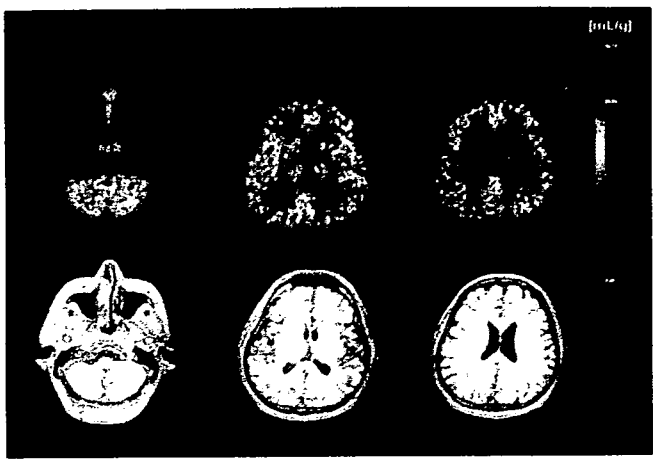

Figure 1. Representative images of the distribution volume of [^{11}C]SA4503-PET at baseline shown with corresponding MRI images. PET, positron emission tomography; MRI, magnetic resonance imaging.

and genotype of the SIGMAR1 gene was analyzed by one-way analysis of variance. Significance for the results was set at $p < .05$.

Results

Radioactivity was distributed throughout the human brain after intravenous administration of [^{11}C]SA4503. Representative parametric images of the distribution volume of [^{11}C]SA4503 at baseline are shown with corresponding MRI images in Figure 1. These results show that sigma-1 receptors are concentrated in brain areas of the limbic system, including areas involved in motor function, sensory perception, and endocrine function, consistent with the previous reports (29,34). Representative images of the distribution volume of [^{11}C]SA4503 in the fluvoxamine- and paroxetine-loading conditions are shown in Figure 2. A single administration of fluvoxamine (200 mg), but not paroxetine (20 mg), markedly decreased the distribution volume of [^{11}C]SA4503 (Figure 2). Table 1 shows the binding potentials and occupancy rates in 9 brain regions. [^{11}C]SA4503 bound throughout the brain, and the cerebellum showed the highest binding potential.

We analyzed whether the effects of fluvoxamine on occupancy of sigma-1 receptors were dose-dependent. Analysis using contrast (polynomial) showed that fluvoxamine significantly and dose-dependently bound to sigma-1 receptors in the frontal cortex ($p < .021$), parietal cortex ($p < .024$), occipital cortex ($p < .011$), head of the caudate nucleus ($p < .012$), thalamus ($p < .008$), and cerebellum ($p < .037$). The dose-dependency also seemed to be operative at the temporal cortex ($p < .069$), anterior cingulate gyrus ($p < .073$), and putamen ($p < .067$), but the correlation at these sites was not statistically significant. There were significant correlations between the blood concentration of fluvoxamine and occupancy in the brain regions (temporal cortex: $r = .62$, $p < .05$; parietal cortex: $r = .70$, $p < .05$; occipital cortex: $r = .63$, $p < .05$; head of the caudate nucleus: $r = .70$, $p < .05$; putamen: $r = .67$, $p < .05$; thalamus: $r = .62$, $p < .05$; cerebellum: $r = .77$, $p < .01$). There were weak correlations between the blood concentration of fluvoxamine and occupancy in the other two regions (frontal cortex; $r = .54$, $.05 < p < .1$; cingulate gyrus; $r = .564$, $.05 < p < .1$). Figure 3 shows representative data for the parietal cortex and cerebellum. There were statistically significant correlations between the sigma-1 receptor occupancy and dose or blood concentration of fluvoxamine in both these brain regions (Figure 3).

Next, we examined whether the SIGMAR1 gene polymorphisms affect the binding potential of sigma-1 receptors in human brain. However, all subjects showed TT genotype at the T-485A site. As for the GC-241-240TT polymorphism, 8 subjects had GC/GC genotype, and 5 subjects had GC/TT genotype, and 2 subjects had TT/TT genotype. There was no association between GC-241-240TT polymorphisms and the baseline binding potentials of sigma-1 receptors in any of the brain regions examined (Supplement 1).

Discussion

The major finding of this study is that, after a single oral administration, fluvoxamine bound to sigma-1 receptors in the living human brain in a dose-dependent manner. To our knowledge, this is the first report demonstrating that fluvoxamine binds to sigma-1 receptors in the living human brain at therapeutic doses, which is consistent with the previous report using rat brain (3). Suhara *et al.* (38) reported a high occupancy (approximately 80%) of serotonin transporters in healthy subjects after a single oral administration of fluvoxamine (50 mg). These results suggest that, at therapeutic doses, fluvoxamine binds to sigma-1 receptors as well as serotonin transporters in the human brain. Taken together, these results suggest that sigma-1 receptors may be involved in the mechanism of the action of fluvoxamine.

A recent study demonstrated that cognitive deficits induced in mice by the N-methyl-D-aspartate receptor antagonist phencyclidine (PCP) could be ameliorated by subsequent subchronic administration of fluvoxamine, and that the effects of fluvoxamine could be antagonized by co-administration of the selective sigma-1 receptor antagonist NE-100 (20). Furthermore, the selective sigma-1 receptor agonist SA4503 and the endogenous sigma-1 receptor agonist dehydroepiandrosterone sulphate could improve PCP-induced cognitive deficits in mice, and the efficacy of SA4503 and dehydroepiandrosterone-sulphate on PCP-in-

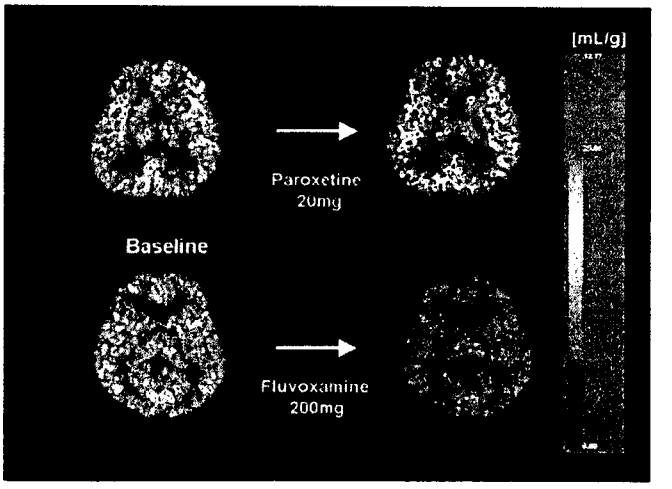

Figure 2. Distribution volume images of [^{11}C]SA4503-PET before and after a single oral administration of an SSRI. The upper pair represents distribution volume images at baseline (left) and at paroxetine (20 mg)-loading (right) in the same subject. The lower pair shows distribution volume images at baseline (left) and fluvoxamine (200 mg)-loading (right) in another subject. PET, positron emission tomography; SSRI, selective serotonin reuptake inhibitor.

Table 1. Binding potential of [^{11}C]SA4503 and occupancy (%) of selective serotonin reuptake inhibitors in the human brain regions

	Frontal Cortex		Temporal Cortex		Parietal Cortex		Occipital Cortex	
	Baseline	SSRI	Baseline	SSRI	Baseline	SSRI	Baseline	SSRI
F50								
Binding potential	15.9±5.2	10.0±3.0	19.5±6.1	14.0±6.0	15.3±4.3	9.57±3.0	14.7±4.8	10.1±4.5
Occupancy (%)	35.5±11.8		27.3±20.0		36.2±13.9		30.8±19.3	
F100								
Binding potential	11.7±3.0	6.56±0.1	14.3±2.6	8.93±2.7	13.6±1.7	7.10±1.2	12.9±0.9	6.69±0.8
Occupancy (%)	41.7±13.0		36.1±22.6		47.0±12.8		48.0±7.3	
F150								
Binding potential	20.9±3.7	7.50±1.2	26.9±4.9	10.0±1.0	20.6±1.9	7.39±0.5	19.2±5.3	6.86±0.3
Occupancy (%)	62.8±12.7		61.7±8.6		63.8±5.9		62.3±10.7	
F200								
Binding potential	17.0±5.1	6.35±0.1	20.8±7.0	9.89±2.9	16.7±4.4	6.27±0.4	15.0±6.0	5.18±1.0
Occupancy (%)	59.9±13.6		50.2±14.9		59.9±14.5		63.0±11.5	
P20								
Binding potential	16.5±2.9	17.1±1.6	20.9±5.6	20.6±1.2	18.4±3.6	15.7±2.2	15.6±3.5	14.8±3.0
Occupancy (%)	−4.40±9.1		−2.2±22.1		13.8±5.6		4.70±4.8	

Value are the mean ± SD of three subjects.

F50, Fluvoxamine (50 mg); F100, fluvoxamine (100 mg); F150, fluvoxamine (150 mg); F200, fluvoxamine (200 mg); P20, paroxetine (20 mg); SSRI, fluvoxamine or paroxetine.

duced cognitive deficits was also antagonized by co-administration of NE-100 (20). These findings suggest that the agonistic activity of fluvoxamine at sigma-1 receptors could be implicated in the mechanisms of the action of fluvoxamine (20). Therefore, the agonistic property of fluvoxamine at sigma-1 receptors may suggest that this drug has potential for the treatment of cognitive deficits in depressive and schizophrenic patients.

Mood disorders, including major depressive disorder and bipolar disorder, possess cognitive impairment in the center of their psychopathology. There is a hypothesis that cognitive dysfunction remains after remission, especially in manic bipolar disorder (39), and leads to poor social outcome. As suggested, fluvoxamine may have a potential for treating cognitive deficits through its action against sigma-1 receptors, it being an antidepressant, fluvoxamine may be a useful prescription for mood disorders having cognitive impairment.

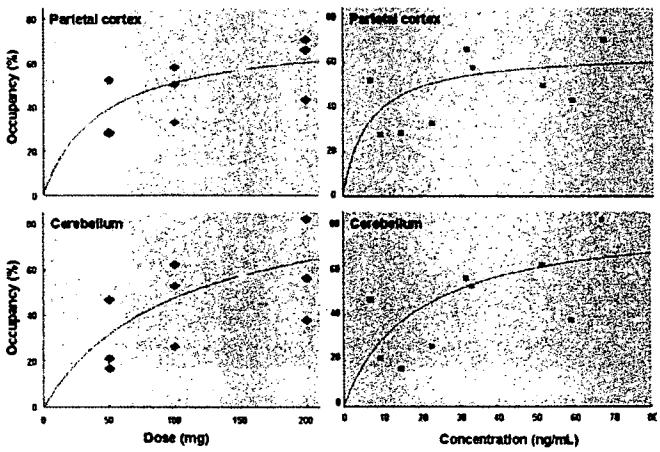

Figure 3. Correlations between the sigma-1 receptor occupancy and dose or blood concentration of fluvoxamine in the parietal cortex and cerebellum. The colors of the points correspond to the dose administered.

An adjunct medication is often added to antipsychotic treatment regimens to improve the response of negative symptoms and cognitive deficits in schizophrenia. Some SSRIs, such as fluvoxamine and fluoxetine, can ameliorate primary negative symptoms in chronic schizophrenic patients (40,41). Currently, the precise mechanism(s) underlying the efficacy of fluvoxamine on negative symptoms is unclear. However, it is possible that sigma-1 receptors play a role in the mechanism of the action of fluvoxamine, although further study will be needed to confirm this. Taken together, these results also suggest that augmentation with sigma-1 receptor agonists such as fluvoxamine could be a useful addition to the treatment of schizophrenic patients with persistent negative symptoms and cognitive deficits.

Psychotic major depression is a difficult-to-treat illness that is associated with high functional impairment and significantly higher mortality than nonpsychotic major depression (42,43). Interestingly, monotherapy of fluvoxamine has been proven effective against both the psychotic and depressive symptoms of this disorder (44–46). In contrast, a monotherapy of paroxetine did not show equal efficacy as fluvoxamine (47). Based on these findings, it has been recently proposed that this efficacy of fluvoxamine might be due to its specific affinity to sigma-1 receptors in the brain (48,49), suggesting that sigma-1 receptors play a role in psychotic major depression. Therefore, it may be interesting to study whether the binding of [^{11}C]SA4503 to sigma-1 receptors in the brain is altered in patients with psychotic major depression.

Miyatake *et al.* (30) reported functional polymorphisms (T-485A) in the promoter region of the SIGMAR1 gene. In this study, we found that there was no association between the SIGMAR1 genotype and the binding potentials of [^{11}C]SA4503 in any of the regions of the brain in healthy male subjects. These findings suggest that the SIGMAR1 gene polymorphism GC-241-240TT may not contribute to differences in the sigma-1 receptors in the human brain, although a further study using a larger sample will be necessary.

In conclusion, the present study demonstrates that fluvoxamine binds to sigma-1 receptors in the human brain at therapeutic

Table 1. (continued)

Anterior Cingulate Gyrus		Head of Caudate Nucleus		Putamen		Thalamus		Cerebellum	
Baseline	SSRI	Baseline	SSRI	Baseline	SSRI	Baseline	SSRI	Baseline	SSRI
18.3±6.1	11.5±2.6	13.8±3.8	9.32±2.2	14.1±4.3	9.06±1.9	16.4±6.4	11.1±3.5	23.5±8.5	16.5±6.5
34.0±17.6		31.2±11.2		34.0±8.8		29.1±15.1		28.2±16.3	
15.3±4.0	8.38±1.4	12.3±0.8	6.19±0.3	12.6±1.5	6.05±0.4	13.7±1.4	8.21±0.4	20.3±6.6	10.1±2.4
40.1±28.9		49.6±1.9		51.7±4.0		39.6±9.1		47.1±18.5	
22.2±3.0	9.23±1.6	17.4±0.4	6.05±2.3	18.6±2.3	7.88±1.3	17.8±1.6	8.57±1.0	29.6±8.5	9.88±1.9
58.1±10.0		65.1±14.2		56.7±12.1		52.4±8.1		65.5±6.9	
19.9±6.0	7.11±1.2	14.3±3.4	5.01±1.0	15.5±5.7	6.11±1.1	14.9±4.4	6.16±1.1	22.8±8.4	8.22±2.4
61.7±14.0		62.1±18.7		55.8±20.5		57.1±8.9		58.5±22.2	
18.0±4.6	18.4±3.8	15.5±2.9	15.0±5.1	16.8±4.4	15.5±1.5	14.7±3.0	15.9±3.1	23.3±6.8	23.7±1.9
−5.20±26.8		5.10±14.4		5.43±14.2		−11.7±35.3		−7.15±28.7	

doses. These findings suggest that sigma-1 receptors may play an important role in the mechanism of action of fluvoxamine. 26,33

This study was supported in part by a grant from the Program for Promotion of Fundamental Studies in Health Sciences of the National Institute of Biomedical Innovation, Japan (to KH and KI, No: 06-46). Dr. Hashimoto reports having received the speakers' bureau honoraria from Solvay Pharmaceuticals. Drs. Ishikawa, Ishiwata, Ishii, Kimura, Sakata, Naganawa, Oda, Miyatake, Fujisaki, Shimizu, Shirayama, and Iyo report no competing interests.

We thank Dr. Masaya Hashimoto and Ms. Hiroko Tsukinari for technical assistance.

Supplementary material cited in this article is available online.

1. Owens MJ (2004): Selectivity of antidepressants: from the monoamine hypothesis of depression to the SSRI revolution and beyond. *J Clin Psychiatry* 65:5–10.
2. Millan ML (2006): Multi-target strategies for the improved treatment of depressive states: Conceptual foundations and neuronal substrates, drug discovery and therapeutic application. *Pharmacol Ther* 110:135–370.
3. Narita N, Hashimoto K, Tomitaka S, Minabe Y (1996): Interactions of selective serotonin reuptake inhibitors with subtypes of sigma receptors in rat brain. *Eur J Pharmacol* 307:117–119.
4. Goodnick PJ, Goldstein BJ (1998): Selective serotonin reuptake inhibitors in affective disorders–I. Basic pharmacology. *J Psychopharmacol* 12:S5–20.
5. Goodnick PJ, Goldstein BJ (1998): Selective serotonin reuptake inhibitors in affective disorders–II. Efficacy and quality of life. *J Psychopharmacol* 12:S21–54.
6. Stahl SM (1998): Not so selective serotonin selective reuptake inhibitors. *J Clin Psychiatry* 59:343–344.
7. Stahl SM (1998): Using secondary binding properties to select a not so selective serotonin selective reuptake inhibitor. *J Clin Psychiatry* 59:642–643.
8. Nemeroff CB, Owens MJ (2004): Pharmacologic differences among the SSRIs: focus on monoamine transporters and the HPA axis. *CNS Spectr* 9:23–31.
9. Bermack JE, Debonnel G (2005): The role of sigma receptors in depression. *J Phamacol Sci* 97:317–336.
10. Carrasco JL, Sandner C (2005): Clinical effects of pharmacological variations in selective serotonin reuptake inhibitors: An overview. *Int J Clin Pract* 59:1428–1434.
11. Westenberg HGM, Sandner C (2006): Tolerability and safety of fluvoxamine and other antidepressants. *Int J Clin Pract* 60:482–491.
12. Walker JM, Bowen WD, Walker FO, Matsumoto RR, De Costa B, Rice KC (1990). Sigma receptors: Biology and function. *Pharmacol Rev* 42:355–402.
13. Maurice T, Urani A, Phan VL, Romieu P (2001): The interaction between neuroactive steroids and the sigma-1 receptor function: Behavioral consequences and therapeutic opportunities. *Brain Res Rev* 37:116–132.
14. Hayashi T, Su TP (2004): Sigma-1 receptor ligands: potential in the treatment of neuropsychiatric disorders. *CNS Drugs* 18:269–284.
15. Hashimoto K, Ishiwata K (2006): Sigma receptor ligands: Possible application as therapeutic drugs and as radiopharmaceuticals. *Curr Pharm Des* 12:3857–3876.
16. Monnet FP, Maurice T (2006): The sigma-1 protein as a target for the nongenomic effects of neuro(active)steroids: Molecular, physiological, and behavioral aspects. *J Pharmacol Sci* 100:93–118.
17. Hayshi T, Su TP (2005): The potential role of sigma-1 receptors in lipid transport and lipid raft reconstitution in the brain: Implication for drug abuse. *Life Sci* 77:1612–1624.
18. Hayashi T, Maurice T, Su TP (2000): Ca^{2+} signaling via sigma-1 receptors: novel regulatory mechanism affecting intracellular Ca^{2+} concentration. *J Pharmacol Exp Ther* 293:788–798.
19. Hayashi T, Su TP (2001): Regulating ankyrin dynamics: Roles of sigma-1 receptors. *Proc Natl Acad Sci U S A* 98:491–496.
20. Hashimoto K, Fujita Y, Iyo M (2007): Phencyclidine-induced cognitive deficits in mice are improved by subsequent subchronic administration of fluvoxamine: Role of sigma-1 receptors. *Neuropsychopharmacology* 32:514–521.
21. Waarde A (2000): Measuring receptor occupancy with PET. *Curr Pharm Des* 6:1593–1610.
22. Kapur S, Seeman P (2001): Does fast dissociation from the dopamine D_2 receptor explain the action of atypical antipsychotics?: A new hypothesis. *Am J Psychiatry* 158:360–369.
23. Kawamura K, Ishiwata K, Tajima H, Ishii S, Matsuno K, Homma Y, *et al.* (2000): In vivo evaluation of [^{11}C]SA4503 as a PET ligand for mapping CNS sigma-1 receptors. *Nucl Med Biol* 27:255–261.
24. Kawamura K, Elsinga PH, Kobayashi T, Ishii S, Wang WF, Matsuno K, *et al.* (2003): Synthesis and evaluation of ^{11}C- and ^{18}F-labeled 1-[2-(4-alkoxy-3-methoxyphenyl)ethyl]-4-(3-phenylpropyl)piperazines as sigma receptor ligands for positron emission tomography studies. *Nucl Med Biol* 30:273–284.

25. Ishiwata K, Tsukada H, Kawamura K, Kimura Y, Nishiyama S, Kobayashi T, *et al.* (2001): Mapping of CNS sigma-1 receptors in the conscious monkey: Preliminary PET study with [^{11}C]SA4503. *Synapse* 40:235–237.
26. Ishiwata K, Kawamura K, Kobayashi T, Matsuno K (2003): Sigma-1 and dopamine D_2 receptor occupancy in the mouse brain after a single administration of haloperidol and two dopamine D_2-like receptor ligands. *Nucl Med Biol* 30:429–434.
27. Matsuno K, Nakazawa M, Okamoto K, Kawashima Y, Mita S (1996): Binding properties of SA4503 a novel and selective sigma1 receptor agonist. *Eur J Pharmacol* 306:271–279.
28. Mishina M, Ishiwata K, Ishii K, Kitamura S, Kimura Y, Kawamura K, *et al.* (2005): Function of sigma-1 receptors in Parkinson's disease. *Acta Neurol Scand* 112:103–107.
29. Ishiwata K, Oda K, Sakata M, Kimura Y, Kawamura K, Oda K, *et al.* (2006): A feasible study of [^{11}C]SA4503-PET for evaluating sigma-1 receptor occupancy by neuroleptics: The binding of haloperidol to sigma-1 and dopamine D_2-like receptors. *Ann Nucl Med* 20:569–573.
30. Miyatake R, Furukawa A, Matsushita S, Higuchi S, Suwaki H (2004): Functional polymorphisms in the sigma-1 receptor gene associated with alcoholism. *Biol Psychiatry* 55:85–90.
31. de Vries MH, Raghoebar M, Mathlener IS, van Harten J (1992): Single and multiple oral dose fluvoxamine kinetics in young and elderly subjects. *Ther Drug Monit* 14:493–498.
32. de Vries MH, van Harten J, van Bemmel P, Raghoebar M (1993): Pharmacokinetics of fluvoxamine maleate after increasing single oral doses in healthy subjects. *Biopharm Drug Dispos* 14:291–296.
33. Fujiwara T, Watanuki S, Yamamoto S, Miyake M, Seo S, Itoh M, *et al.* (1997): Performance evaluation of a large axial field-of-view PET scanner: SET-2400W. *Ann Nucl Med* 11:307–313.
34. Sakata M, Kimura Y, Naganawa M, Oda K, Ishii K, Chihara K, *et al.* (2007): Mapping of human cerebral sigma-1 receptors using positron emission tomography and [^{11}C]SA4503. *Neuroimage* 35:1–8.
35. Mintun MA, Raichle ME, Kilbourn MR, Wooten GF, Welch MJ (1984): A quantitative model for the in vivo assessment of drug binding sites with positron emission tomography. *Ann Neurol* 15:217–227.
36. Logan J, Fowler JS, Volkow ND, Wang GJ, Ding YS, Alexoff DL (1996): Distribution volume ratios without blood sampling from graphical analysis of PET data. *J Cereb Blood Flow Metab* 16:834–840.
37. Ishiguro H, Ohtsuki T, Toru M, Itokawa M, Aoki J, Shibuya H, *et al.* (1998): Association between polymorphisms in the type 1 sigma receptor gene and schizophrenia. *Neurosci Lett* 257:45–48.
38. Suhara T, Takano A, Sudo Y, Ichimiya T, Inoue M, Yasuno F, *et al.* (2003): High levels of serotonin transporter occupancy with low-dose clomipramine in comparative occupancy study with fluvoxamine using positron emission tomography. *Arch Gen Psychiatry* 60:386–391.
39. Gruber S, Rathgeber K, Braunig P, Gauggel S (2007): Stability and course of neuropsychological deficits in manic and depressed bipolar patients compared to patients with major depression. *J Affect Disord* Mar 13; [Epub ahead of print].
40. Silver H (2003): Selective serotonin reuptake inhibitor augmentation in the treatment of negative symptoms of schizophrenia. *Int Clin Psychopharmacol* 18:305–313.
41. Silver H (2004): Selective serotonin re-uptake inhibitor augmentation in the treatment of negative symptoms of schizophrenia. *Expert Opin Pharmacother* 5:2053–2058.
42. Schatzberg AF (2003): New approaches to managing psychotic depression. *J Clin Psychiatry* 64:19–23.
43. Vythilingam M, Chen J, Bremner JD, Mazure CM, Maciejewski PK, Nelson JC (2003): Psychotic depression and mortality. *Am J Psychiatry* 160:574–576.
44. Gatti F, Bellini L, Gasperini M, Perez J, Zanardi R, Smeraldi E (1996): Fluvoxamine alone in the treatment of delusional depression. *Am J Psychiatry* 153:414–416.
45. Hirschfeld RM (1999): Efficacy of SSRIs and newer antidepressants in severe depression: Comparison with TCAs. *J Clin Psychiatry* 60:326–335.
46. Zanardi R, Franchini L, Gasperini M, Lucca A, Smeraldi E, Perez J (1998): Faster onset of action of fluvoxamine in combination with pindolol in the treatment of delusional depression: A controlled study. *J Clin Psychopharmacol* 18:441–446.
47. Zanardi R, Franchini L, Gasperini M, Perez J, Smeraldi E (1996): Double-blind controlled trial of sertraline versus paroxetine in the treatment of delusional depression. *Am J Psychiatry* 153:1631–1633.
48. Stahl SM (2005): Antidepressant treatment of psychotic major depression: Potential role of the σ receptor. *CNS Spectr* 10:319–323.
49. Hayashi T, Su TP (2005): Understanding the role of sigma-1 receptors in psychotic depression. *Psychiatric Times* 22:54–63.

Evaluation of Distribution of Adenosine A_{2A} Receptors in Normal Human Brain Measured With [^{11}C]TMSX PET

MASAHIRO MISHINA,[1,2,3]* KIICHI ISHIWATA,[2] YUICHI KIMURA,[2] MIKA NAGANAWA,[2,4] KEIICHI ODA,[2] SHIRO KOBAYASHI,[1] YASUO KATAYAMA,[3] AND KENJI ISHII[2]

[1]*Neurological Institute, Nippon Medical School Chiba-Hokusoh Hospital, Imba-gun, Chiba-ken 270-1694, Japan*
[2]*Positron Medical Center, Tokyo Metropolitan Institute of Gerontology, Itabashi-ku, Tokyo 173-0022, Japan*
[3]*The Second Department of Internal Medicine, Nippon Medical School, Bunkyo-ku, Tokyo 113-8602, Japan*
[4]*JSPS Research Fellow, Japan Society for the Promotion of Science, Chiyoda-ku, Tokyo 102-8471, Japan*

KEY WORDS adenosine A_{2A} receptor; positron emission tomography; [^{11}C]TMSX; human brain; Parkinson's disease

ABSTRACT Adenosine A_{2A} receptor (A2AR) is thought to interact with dopamine D_2 receptor. Selective A2AR antagonists have attracted attention as the treatment of Parkinson's disease. In this study, we investigated the distribution of the A2ARs in the living human brain using positron emission tomography (PET) and [7-methyl-^{11}C]-(*E*)-8-(3,4,5-trimethoxystyryl)-1,3,7-trimethylxanthine ([^{11}C]TMSX). We recruited five normal male subjects. A dynamic series of PET scans was performed for 60 min, and the arterial blood was sampled during the scan to measure radioactivity of the parent compound and labeled metabolites. Circular regions of interest of 10-mm diameter were placed in the PET images over the cerebellum, brainstem, thalamus, head of caudate nucleus, anterior and posterior putamen, frontal lobe, temporal lobe, parietal lobe, occipital lobe, and posterior cingulate gyrus for each subject. A two-tissue, three-compartment model was used to estimate K_1, k_2, k_3, and k_4 between metabolite-corrected plasma and tissue time activity of [^{11}C]TMSX. The binding potential (BP) was the largest in the anterior (1.25) and posterior putamen (1.20), was next largest in the head of caudate nucleus (1.05) and thalamus (1.03), and was small in the cerebral cortex, especially frontal lobe (0.46). [^{11}C]TMSX PET showed the largest BP in the striatum in which A2ARs were enriched as in postmortem and nonhuman studies reported, but that the binding of [^{11}C]TMSX was relatively larger in the thalamus to compare with other mammals. To date, [^{11}C]TMSX is the only promising PET ligand, which is available to clinical use for mapping the A2ARs in the living human brain. **Synapse 61:778–784, 2007.** © 2007 Wiley-Liss, Inc.

INTRODUCTION

Adenosine is produced by conversion of intra- and extracellular adenine nucleotides (Latini and Pedata, 2001), and plays a role as an endogenous modulator of synaptic functions in the central nervous system (Dunwiddie and Masino, 2001). The effects are mediated by at least four receptor subtypes: A_1, A_{2A}, A_{2B}, and A_3 (Fredholm et al., 2001). The adenosine A_{2A} receptors are enriched in dopamine-rich areas of the brain, such as the basal ganglia (Fredholm and Svenningsson, 2003), while adenosine A_1 receptors are widely distributed throughout the entire brain (Fukumitsu et al., 2005). The adenosine A_{2A} receptors are known to stimulate adenyl cyclase and would interact with dopamine D_2 receptor negatively at the level of second messengers and beyond (Fredholm and Svenningsson, 2003). For example, high-affinity binding of a dopamine D_2 agonist could be reduced by stimulation of adenosine A_{2A} receptors (Ferre et al., 1991).

Recently, adenosine A_{2A} receptor antagonists have attracted attention as the nondopaminergic treatment of Parkinson's disease. Caffeine is a nonselective adenosine receptor antagonist and is known to reduce the risk of developing Parkinson's disease (Ascherio et al., 2001; Ross et al., 2000). Theophylline, which is also a nonselective antagonist, was expected as a promising

Contract grant sponsor: Japan Society for the Promotion of Science; Contract grant numbers: No 16390348, No. 17590901.

*Correspondence to: Masahiro Mishina, MD, Neurological Institute, Nippon Medical School Chiba-Hokusoh Hospital, 1715 Kamagari, Imba-mura, Imba-gun, Chiba-ken 270-1694, Japan. E-mail: mishina@nms.ac.jp

Received 17 November 2006; Accepted 26 March 2007

DOI 10.1002/syn.20423

Published online 13 June 2007 in Wiley InterScience (www.interscience.wiley.com).

© 2007 WILEY-LISS, INC.

WILEY InterScience® DISCOVER SOMETHING GREAT

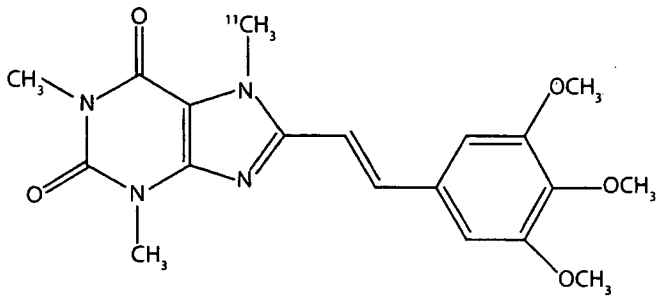

Fig. 1. Chemical structure of [^{11}C]TMSX.

agent of Parkinson's disease (Kostic et al., 1999). However, clinical trials of the caffeine and theophylline have been unimpressive (Kulisevsky et al., 2002; Schwarzschild et al., 2002). The selective adenosine A_{2A} receptor antagonist, istradefylline (KW6002), has been developed as a novel nondopaminergic agent for Parkinson's disease (Kase, 2001), and provides an antiparkinsonian benefit without causing and worsening dyskinesia that is one of the most inconvenient side effects of dopaminergic therapy (Bara-Jimenez et al., 2003). A postmortem study suggested that adenosine A_{2A} receptors was increased in the patients with dyskinesia following long-term levodopa therapy (Calon et al., 2004). Therefore, adenosine A_{2A} receptors may be involved with the appearance of the side effects of the antiparkinsonian agents.

Although adenosine A_{2A} receptor has attracted much attention, little information was available about the receptor in the living human brain until quite recently. However, we developed a PET ligand, [7-methyl-^{11}C]-(*E*)-8-(3,4,5-trimethoxystyryl)-1,3,7-trimethylxanthine ([^{11}C]TMSX, Fig. 1), for mapping the adenosine A_{2A} receptors (Ishiwata et al., 2000a,b, 2002). Preliminarily, we have successfully visualized the receptors in a living human brain in comparison with distribution of adenosine A_1 receptors and dopamine D_2 receptors, and the receptor-specific binding of [^{11}C]TMSX was confirmed by theophylline challenge (Ishiwata et al., 2005). The aim of this study is to establish the measurement of the adenosine A_{2A} receptors in the living human brain using the [^{11}C]TMSX PET, and to compare with the results of past postmortem and nonhuman studies.

MATERIALS AND METHODS

Subjects

We recruited five-normal male subjects, without the history of neurological disease or any abnormalities on physical or neurological examinations (mean age ± SD, 23.0 ± 3.3). They were all right-handed. They had neither medication known to affect the brain function nor history of alcoholism.

The study protocols were approved by the Ethics Committee of Tokyo Metropolitan Institute of Gerontology. A written informed consent was obtained from all of the subjects who participated in this study.

Magnetic resonance imaging

Magnetic resonance images (MRI) were obtained with the spoiled gradient-recalled echo in steady state technique and a SIGNA 1.5 Tesla machine (General Electric, Waukesha, WI). MRI images were examined for any organic abnormalities in the subjects' brain, and were used as a reference for placing regions of interest (ROIs) on PET images.

Positron emission tomography imaging

PET was performed in the Tokyo Metropolitan Institute of Gerontology Positron Medical Center with an SET-2400W PET scanner (Shimadzu Co., Kyoto, Japan) (Fujiwara et al., 1997). [^{11}C]TMSX was prepared as described before (Ishiwata et al., 2003). Specific activity at the time of injection ranged from 12.8 to 48.9 GBq/μmol (27.4 ± 14.5 GBq/μmol). After transmission scan with a rotating ^{68}Ga/^{68}Ge line source to correct for the photon attenuation using the attenuation map, a dynamic series of decay-corrected PET data acquisition was performed for 60 min starting at the time of 500 MBq of [^{11}C]TMSX injection. The total number of frames was 27, and the frame arrangements were 10 s × 6, 30 s × 3, 1 min × 5, 2.5 min × 5, 5 min × 8. Arterial blood was sampled at 10, 20, 30, 40, 50, 60, 70, 80, 90, 100, 110, 120, 135, and 150 s, and at 3, 5, 7, 10, 15, 20, 30, 40, 50, and 60 min. Plasma was separated, weighed, and measured for radioactivity with an NaI (Tl) well scintillation counter. Metabolite analysis was carried out by high-performance liquid chromatography (HPLC). The time activity curves in plasma (pTAC) were expressed as standardized uptake value (SUV, [Bq/ml tissue]/[Bq dose/g body weight]). All procedures were performed under dim light to prevent photoisomerization of the TMSX (Ishiwata et al., 1996, 2000a, 2003).

Kinetic analysis

We generated early images by adding up frames of the dynamic scan from 0 to 10 min (Mishina et al., 2000). The MRI was three-dimensionally registered to the early image of each subject using the K-means clustering algorithm (Ardekani et al., 1995). Using a medical image processing application package "Dr. View" version 5.2 (AJS Co., Tokyo, Japan), the early images and the registered MRI images were used as a reference for placing ROIs on PET image of dynamic scans (Fig. 2). Circular ROIs of 10-mm diameter and extending over two slices of the PET images were drawn on the cerebellum, brainstem, thalamus, head of caudate nucleus, anterior and posterior putamen, frontal lobe, temporal lobe, parietal lobe, occipital lobe, and posterior cingulate gyrus. We also placed the ROIs

Fig. 2. Placement of regions of interest using Dr. View. Using the software, we can place the same ROIs on the images of different modalities.

over the centrum semiovale on one slice as a reference region for kinetic analysis. Time activity curves in tissue (tTACs) were calculated as SUV with the dynamic data and ROIs. A kinetic analysis of the tTACs was performed using programs implemented on MATLAB 7.04 (The Mathworks, Natick, MA). The metabolite-corrected pTAC was used as an input function. A two-tissue, three-compartment model was used to estimate K_1, k_2, k_3, and k_4 between pTAC and tTAC of [^{11}C]TMSX using Gauss-Newton algorithm (Kawamura et al., 2003) and a tTAC of the centrum semiovale. Estimation of delay was performed in a round-robin fashion (Kimura et al., 2004). Then, total distribution volume (DVt), $\frac{K_1}{k_2}\left(1+\frac{k_3}{k_4}\right)$, and binding potential (BP), $\frac{k_3}{k_4}$, were calculated using the parameters. Rate of specific binding (SB) was calculated as $\frac{BP}{DVt}$. Parametric images of DVt for [^{11}C]TMSX were also generated using a graphical analysis (Logan, 2003). Rationale of the kinetic analysis was validated in detail by Naganawa et al. (2007).

RESULTS

Figure 3 demonstrate the curve for the unmetabolized [^{11}C]TMSX and the unmetabolized ratio of [^{11}C]TMSX in plasma, respectively. The radioactivity level in plasma rapidly decreased for the first 5 min (Fig. 3A). [^{11}C]TMSX was metabolically stable in plasma, and over 90% of the radioactivity remained as the intact form for 60 min (Fig. 3B).

Figure 4 demonstrates the time radioactivity curve in the putamen, frontal cortex, and centrum semiovale. [^{11}C]TMSX was taken at high level, and the uptake reached a peak at 1.5–2.5 min after injection, followed by a gradual decrease. The SUV was large in the putamen and small in the frontal lobe.

Figure 5 shows representative parametric images for the DVt of [^{11}C]TMSX. The images demonstrate that the DVt was high in the putamen, head of caudate nucleus and thalamus, and was low in the cerebral cortex.

The BP was large in the anterior and posterior putamen, head of caudate nucleus and thalamus, was moderate in the cerebellum and brainstem, and was small in the cerebral cortices, especially frontal lobe (Table I). The rate of specific binding was 62% in the putamen and 38% in the frontal cortex (Table I).

DISCUSSION

Our study demonstrated that adenosine A_{2A} receptors in human brain were enriched in the striatum, as

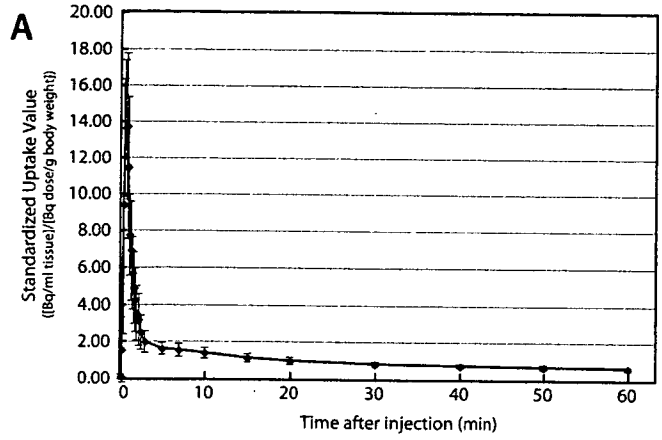

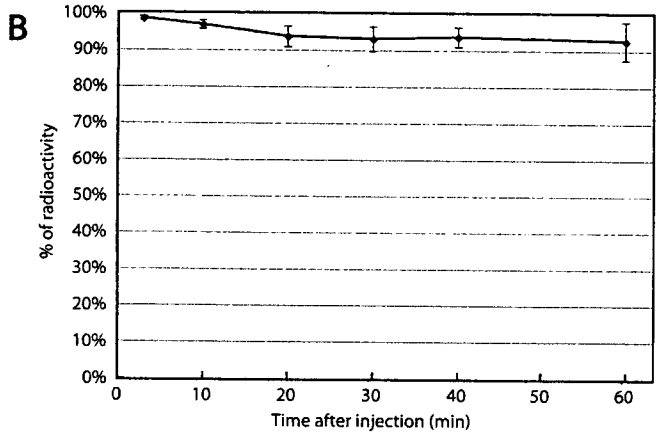

Fig. 3. Decay-corrected time–radioactivity curve for unmetabolized [^{11}C]TMSX in plasma (**A**) and unmetabolized ratio of [^{11}C]TMSX (**B**). Data represent means and SD of five subjects.

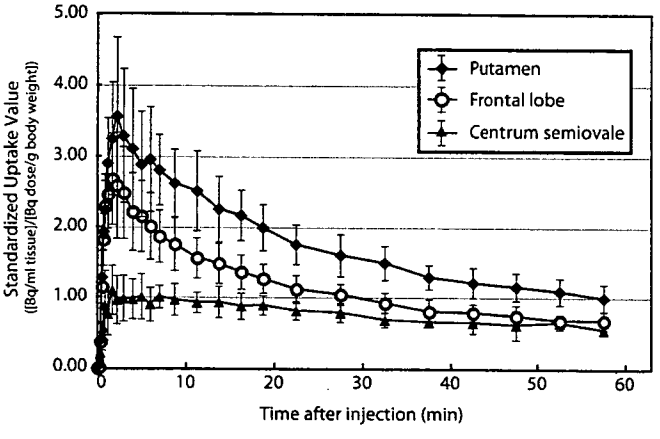

Fig. 4. Decay-corrected time–radioactivity curve for unmetabolized [^{11}C]TMSX in the putamen, frontal cortex, and centrum semiovale for five normal subjects.

well as human postmortem studies (Martinez-Mir et al., 1991; Svenningsson et al., 1997). Among the mouse, rat, and monkey studies using [^{11}C]TMSX (Ishiwata et al., 2000a) and [^{11}C]SCH44241 (Moresco et al., 2005), which is also a selective adenosine A_{2A} receptor antagonist, the uptake of the tracer was higher in the striatum than in the other brain region. The findings are coincident with the fact that the adenosine A_{2A} receptors are enriched in the striatum in all species.

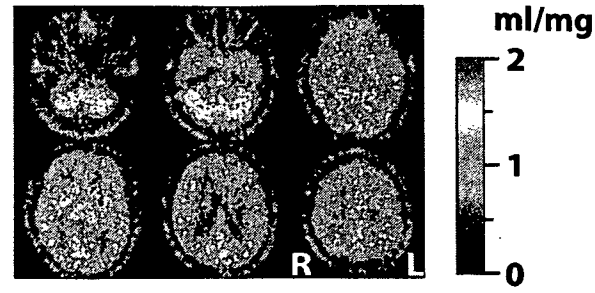

Fig. 5. A parametric image for the total distribution volume of [^{11}C]TMSX generated using a graphical analysis. This image is including the nonspecific binding of TMSX. The image demonstrate that the distribution of [^{11}C]TMSX was high in the putamen, head of caudate nucleus and thalamus, and low in the cerebral cortex.

TABLE I. Total distribution volume, binding potential, and rate of specific binding of [^{11}C]TMSX

	DVt (ml/mg)	BP	SB (%)
Cerebellum	1.39 ± 0.34	0.85 ± 0.15	53.0 ± 2.8
Brainstem	1.33 ± 0.31	0.77 ± 0.13	50.7 ± 3.3
Thalamus	1.53 ± 0.37	1.03 ± 0.13	58.0 ± 1.8
Caudate nucleus	1.55 ± 0.36	1.05 ± 0.17	58.4 ± 3.5
Anterior putamen	1.69 ± 0.38	1.25 ± 0.17	62.7 ± 3.5
Posterior putamen	1.66 ± 0.41	1.20 ± 0.16	61.8 ± 2.3
Frontal lobe	1.10 ± 0.27	0.46 ± 0.11	37.8 ± 3.3
Temporal lobe	1.16 ± 0.27	0.54 ± 0.11	42.1 ± 3.5
Occipital lobe	1.17 ± 0.26	0.56 ± 0.10	42.7 ± 3.9
Parietal lobe	1.14 ± 0.26	0.51 ± 0.10	40.6 ± 3.3
Posterior cingulate gyrus	1.29 ± 0.30	0.72 ± 0.14	49.0 ± 4.0

DVt = total distribution volume, BP = binding potential, SB = rate of specific binding.

Our study showed that the distribution of the adenosine A_{2A} receptors were widespread other than in striatum. Following in the putamen and head of caudate nucleus, the BP of [^{11}C]TMSX was the largest in the thalamus. The BP was smaller in the cerebral cortex, especially frontal lobe, than in the cerebellum. Table II summarizes previous works for bindings pf radioligands to adenosine A_{2A} receptors in experimental animals. [^{11}C]TMSX uptake was lower in the cerebral cortex than in the cerebellum (Ishiwata et al., 2000a). The animal study using [^{11}C]SCH44241 reported, however, that the uptake was higher in the cerebral cortex than in the cerebellum (Moresco et al., 2005). The postmortem study revealed that the density of adenosine A_{2A} receptors in the putamen and caudate nucleus was five times of that in the thalamus, and was 3~5 times of those in the cortices (Svenningsson et al., 1997). Our result showed, however, that the BP of [^{11}C]TMSX in the putamen was 1.2

TABLE II. Summary of past studies on the binding of radioligands to adenosine A_{2A} receptors

Description							Reference
	Uptake ratio				BP (mean ± SD)	B_{MAX} ± SEM (fmol/mg)	
	5 min	15 min	30 min	60 min			
[^{11}C]TMSX							
Mouse: in vitro autoradiography							
Striatum/cortex	2.32	2.82	2.85	2.53			Ishiwata et al., 2000a*
Striatum/cerebellum	2.08	2.71	2.64	2.55			
Rat: in vitro autoradiography							
Striatum/cortex		3.16					
Striatum/cerebellum		2.67					
Monkey: PET							
Striatum/cortex	1.30	1.40	1.47	1.56			
Striatum/cerebellum	1.20	1.22	1.26	1.46			
[^{11}C]SCH44241							
Monkey: PET							
Striatum					0.74 ± 0.02		Moresco et al., 2005
Cortex					0.16 ± 0.04		
Cerebellum					0.13 ± 0.06		
[^{3}H]SCH58261							
Postmorten human: in vitro autoradiography							
Rostral putamen						15.0 ± 1.5	Svenningsson et al., 1997
Caudal putamen						11.2 ± 0.9	
Frontal cortex						5.2 ± 0.8	
Occiptal cortex						3.4 ± 1.0	
Medial nucleus of thalamus						3.7 ± 1.0	

*[^{11}C]TMSX was denoted as [^{11}C]KF18446.

times of that in the thalamus, and was 3.7 times of that in the frontal cortex. Our result demonstrated that the BP was smaller in the frontal lobe than in the temporal, occipital, and parietal lobes, although the postmortem study reported that the [^{3}H]SCH58261 binging in the frontal lobe was 1.5 times of those in the temporal and occipital lobes. Taken together these finding, imaging by [^{11}C]TMSX PET reflects distribution of adenosine A_{2A} receptors previously reported, although regional differences in the signals of specific binding of [^{11}C]TMSX were relatively small compared with those of other radioligands. The difference of results may be involved in methodology, such as species, tracer, autoradiography and anesthesia. To investigate the reason of the difference, further studies of living human brain will be needed using other PET ligand, such as [^{11}C]KF21213 (Wang et al., 2000) and [^{11}C]SCH44241 (Todde et al., 2000). Unfortunately, no data are available on the PET ligand for adenosine A_{2A} receptors in living human brain other than [^{11}C]TMSX (Ishiwata et al., 2005).

Past studies proved a functional interaction between adenosine A_{2A} and dopamine D_2 receptors (Fredholm and Svenningsson, 2003). Adenosine A_{2A} receptor is known to be concerned with not only modulation of dopamine, but also that of GABA and glutamate (Mori and Shindou, 2003; Popoli et al., 2003). Our human study showed that adenosine A_{2A} receptors are enriched in dopamine-rich areas, but that the receptors are also distributed in other regions as well as past studies. The adenosine A_{2A} receptors other than classical receptors modulating dopamine are called as "atypical adenosine A_{2A} receptor" (Ishiwata et al., 2000a; Lindstrom et al., 1996). The atypical adenosine A_{2A} receptors may be involved in the cerebral cortex, cerebellum, and thalamus.

In the study of [^{11}C]SCH44241 in monkey (Moresco et al., 2005), the BP was calculated using reference tissue model using the cerebellum as a reference region (Gunn et al., 1997). However, this article also showed that the binding of [^{11}C]SCH44241 was reduced by the administration of KW6002 not only in the striatum but also in the cortex and cerebellum. The result indicated the existence of the specific binding to adenosine A_{2A} receptor in the cerebellum, and the cerebellum is not an ideal reference region. Our data showed that specific binding was over 30% in the human cerebellum, cerebral cortex, and thalamus. In the human [^{11}C]TMSX PET, reference tissue model cannot be applied to calculation of BP with the region of interest (ROI) value of cerebellum, cerebral cortex and thalamus. The centrum semiovale is the region with lowest [^{11}C]TMSX binding, and was considered to be devoid of specific binding, because few neurons exist there. In our kinetic analysis, therefore, we used the ROIs over the centrum semiovale as a reference region (Naganawa et al., 2007).

In the animal study, percentage of unchanged [^{11}C]TMSX in plasma was 80.8% at 30 min in mice, and 41.7% at 30 min and 28.7% at 60 min in a monkey (Ishiwata et al., 2000a). To compare with the monkey, peripheral degradation of [^{11}C]TMSX was very slow in humans. The labeled metabolites may be negligible in the human [^{11}C]TMSX PET examination.

We are interested in human pathological condition of adenosine A_{2A} receptors, especially Parkinson's disease. As stated above, selective adenosine A_{2A} receptor antagonists are promising antiparkinsonian agents (Bara-Jimenez et al., 2003; Hauser et al., 2003). A postmortem study suggested that the density of adenosine A_{2A} receptors was increased in striatopallidal pathway neurons of Parkinson's disease with dyskinesias following long-term levodopa therapy (Calon et al., 2004). To date, clinical evidence is lacking about adenosine A_{2A} receptors of drug naive Parkinson's disease and its alteration after antiparkinsonian treatment. We expect that application of [^{11}C]TMSX PET will demonstrate the unknown mechanism of side effects of antiparkinsonian agents.

In conclusion, [^{11}C]TMSX PET demonstrated that adenosine A_{2A} receptors are enriched in the striatum, as well as postmortem and animal studies reported. However, the human distribution of the adenosine A_{2A} receptor is larger in the thalamus and cerebellum to compare with other mammals. To date, [^{11}C]TMSX is the only promising PET ligand, which is available to clinical use for mapping the adenosine A_{2A} receptors in the living human brain.

ACKNOWLEDGMENTS

The authors thank Dr. T. Oda for production of [^{11}C]TMSX; Ms. H. Tsukinari taking care of the subjects undergoing PET scanning.

REFERENCES

Ardekani BA, Braun M, Hutton BF, Kanno I, Iida H. 1995. A fully automatic multimodality image registration algorithm. J Comput Assist Tomogr 19(4):615–623.

Ascherio A, Zhang SM, Hernan MA, Kawachi I, Colditz GA, Speizer FE, Willett WC. 2001. Prospective study of caffeine consumption and risk of Parkinson's disease in men and women. Ann Neurol 50(1):56–63.

Bara-Jimenez W, Sherzai A, Dimitrova T, Favit A, Bibbiani F, Gillespie M, Morris MJ, Mouradian MM, Chase TN. 2003. Adenosine A_{2A} receptor antagonist treatment of Parkinson's disease. Neurology 61(3):293–296.

Calon F, Dridi M, Hornykiewicz O, Bedard PJ, Rajput AH, Di Paolo T. 2004. Increased adenosine A_{2A} receptors in the brain of Parkinson's disease patients with dyskinesias. Brain 127:1075–1084.

Dunwiddie TV, Masino SA. 2001. The role and regulation of adenosine in the central nervous system. Annu Rev Neurosci 24:31–55.

Ferre S, von Euler G, Johansson B, Fredholm BB, Fuxe K. 1991. Stimulation of high-affinity adenosine A_2 receptors decreases the affinity of dopamine D_2 receptors in rat striatal membranes. Proc Natl Acad Sci USA 88(16):7238–7241.

Fredholm BB, Svenningsson P. 2003. Adenosine-dopamine interactions: Development of a concept and some comments on therapeutic possibilities. Neurology 61(Suppl):S5–S9.

Fredholm BB, IJzerman AP, Jacobson KA, Klotz KN, Linden J. 2001. International Union of Pharmacology. XXV. Nomenclature and classification of adenosine receptors. Pharmacol Rev 53(4): 527–552.

Fujiwara T, Watanuki S, Yamamoto S, Miyake M, Seo S, Itoh M, Ishii K, Orihara H, Fukuda H, Satoh T, Kitamura K, Tanaka K, Takahashi S. 1997. Performance evaluation of a large axial field-of-view PET scanner: SET-2400W. Ann Nucl Med 11(4):307–313.

Fukumitsu N, Ishii K, Kimura Y, Oda K, Sasaki T, Mori Y, Ishiwata K. 2005. Adenosine A_1 receptor mapping of the human brain by PET with 8-dicyclopropylmethyl-1-^{11}C-methyl-3-propylxanthine. J Nucl Med 46(1):32–37.

Gunn RN, Lammertsma AA, Hume SP, Cunningham VJ. 1997. Parametric imaging of ligand-receptor binding in PET using a simplified reference region model. NeuroImage 6(4):279–287.

Hauser RA, Hubble JP, Truong DD. 2003. Randomized trial of the adenosine A_{2A} receptor antagonist istradefylline in advanced PD. Neurology 61(3):297–303.

Ishiwata K, Noguchi J, Toyama H, Sakiyama Y, Koike N, Ishii S, Oda K, Endo K, Suzuki F, Senda M. 1996. Synthesis and preliminary evaluation of [^{11}C]KF17837, a selective adenosine A_{2A} antagonist. Appl Radiat Isot 47(5/6):507–511.

Ishiwata K, Noguchi J, Wakabayashi S, Shimada J, Ogi N, Nariai T, Tanaka A, Endo K, Suzuki F, Senda M. 2000a. ^{11}C-labeled KF18446: A potential central nervous system adenosine A_{2A} receptor ligand. J Nucl Med 41(2):345–354.

Ishiwata K, Ogi N, Shimada J, Nonaka H, Tanaka A, Suzuki F, Senda M. 2000b. Further characterization of a CNS adenosine A_{2A} receptor ligand [^{11}C]KF18446 with in vitro autoradiography and in vivo tissue uptake. Ann Nucl Med 14(2):81–89.

Ishiwata K, Ogi N, Hayakawa N, Oda K, Nagaoka T, Toyama H, Suzuki F, Endo K, Tanaka A, Senda M. 2002. Adenosine A_{2A} receptor imaging with [^{11}C]KF18446 PET in the rat brain after quinolinic acid lesion: Comparison with the dopamine receptor imaging. Ann Nucl Med 16(7):467–475.

Ishiwata K, Wang WF, Kimura Y, Kawamura K, Ishii K. 2003. Preclinical studies on [^{11}C]TMSX for mapping adenosine A_{2A} receptors by positron emission tomography. Ann Nucl Med 17(3):205–211.

Ishiwata K, Mishina M, Kimura Y, Oda K, Sasaki T, Ishii K. 2005. First visualization of adenosine A_{2A} receptors in the human brain by positron emission tomography with [^{11}C]TMSX. Synapse 55(2): 133–136.

Kase H. 2001. New aspects of physiological and pathophysiological functions of adenosine A_{2A} receptor in basal ganglia. Biosci Biotechnol Biochem 65(7):1447–1457.

Kawamura K, Kimura Y, Tsukada H, Kobayashi T, Nishiyama S, Kakiuchi T, Ohba H, Harada N, Matsuno K, Ishii K, Ishiwata K. 2003. An increase of sigma receptors in the aged monkey brain. Neurobiol Aging 24(5):745–752.

Kimura Y, Ishii K, Fukumitsu N, Oda K, Sasaki T, Kawamura K, Ishiwata K. 2004. Quantitative analysis of adenosine A_1 receptors in human brain using positron emission tomography and [1-methyl-^{11}C]8-dicyclopropylmethyl-1-methyl-3-propylxanthine. Nucl Med Biol 31(8):975–981.

Kostic VS, Svetel M, Sternic N, Dragasevic N, Przedborski S. 1999. Theophylline increases "on" time in advanced parkinsonian patients. Neurology 52(9):1916.

Kulisevsky J, Barbanoj M, Gironell A, Antonijoan R, Casas M, Pascual-Sedano B. 2002. A double-blind crossover, placebo-controlled study of the adenosine A_{2A} antagonist theophylline in Parkinson's disease. Clin Neuropharmacol 25(1):25–31.

Latini S, Pedata F. 2001. Adenosine in the central nervous system: Release mechanisms and extracellular concentrations. J Neurochem 79(3):463–484.

Lindstrom K, Ongini E, Fredholm BB. 1996. The selective adenosine A_{2A} receptor antagonist SCH 58261 discriminates between two different binding sites for [^{3}H]-CGS 21680 in the rat brain. Naunyn Schmiedebergs Arch Pharmacol 354(4):539–541.

Logan J. 2003. A review of graphical methods for tracer studies and strategies to reduce bias. Nucl Med Biol 30(8):833–844.

Martinez-Mir MI, Probst A, Palacios JM. 1991. Adenosine A_2 receptors: Selective localization in the human basal ganglia and alterations with disease. Neuroscience 42(3):697–706.

Mishina M, Senda M, Kimura Y, Toyama H, Ishiwata K, Ohyama M, Nariai T, Ishii K, Oda K, Sasaki T, Kitamura S, Katayama Y. 2000. Intrasubject correlation between static scan and distribution volume images for [^{11}C]flumazenil PET. Ann Nucl Med 14(3):193–198.

Moresco RM, Todde S, Belloli S, Simonelli P, Panzacchi A, Rigamonti M, Galli-Kienle M, Fazio F. 2005. In vivo imaging of adenosine A_{2A} receptors in rat and primate brain using [^{11}C]SCH442416. Eur J Nucl Med Mol Imaging 32(4):405–413.

Mori A, Shindou T. 2003. Modulation of GABAergic transmission in the striatopallidal system by adenosine A_{2A} receptors: A potential mechanism for the antiparkinsonian effects of A_{2A} antagonists. Neurology 61(Suppl):S44–S48.

Naganawa M, Kimura Y, Mishina M, Manabe Y, Chihara K, Oda K, Ishii K, Ishiwata K. 2007. Quantification of adenosine A_{2A} receptors in the human brain using [^{11}C]TMSX and positron emission tomography. Eur J Nucl Med 34:679–687.

Popoli P, Frank C, Tebano MT, Potenza RL, Pintor A, Domenici MR, Nazzicone V, Pezzola A, Reggio R. 2003. Modulation of glutamate release and excitotoxicity by adenosine A2A receptors. Neurology 61(Suppl):S69–S71.

Ross GW, Abbott RD, Petrovitch H, Morens DM, Grandinetti A, Tung KH, Tanner CM, Masaki KH, Blanchette PL, Curb JD, Popper JS, White LR. 2000. Association of coffee and caffeine intake with the risk of Parkinson disease. JAMA 283(20):2674–2679.

Schwarzschild MA, Chen JF, Ascherio A. 2002. Caffeinated clues and the promise of adenosine A_{2A} antagonists in PD. Neurology 58(8):1154–1160.

Svenningsson P, Hall H, Sedvall G, Fredholm BB. 1997. Distribution of adenosine receptors in the postmortem human brain: An extended autoradiographic study. Synapse 27(4):322–335.

Todde S, Moresco RM, Simonelli P, Baraldi PG, Cacciari B, Spalluto G, Varani K, Monopoli A, Matarrese M, Carpinelli A, Magni F, Kienle MG, Fazio F. 2000. Design, radiosynthesis, and biodistribution of a new potent and selective ligand for in vivo imaging of the adenosine A_{2A} receptor system using positron emission tomography. J Med Chem 43(23):4359–4362.

Wang WF, Ishiwata K, Nonaka H, Ishii S, Kiyosawa M, Shimada J, Suzuki F, Senda M. 2000. Carbon-11-labeled KF21213: A highly selective ligand for mapping CNS adenosine A_{2A} receptors with positron emission tomography. Nucl Med Biol 27(6):541–546.

ELSEVIER

NeuroImage

www.elsevier.com/locate/ynimg
NeuroImage 35 (2007) 1–8

Mapping of human cerebral sigma$_1$ receptors using positron emission tomography and [^{11}C]SA4503

Muneyuki Sakata,[a] Yuichi Kimura,[b,*] Mika Naganawa,[b,c] Keiichi Oda,[b] Kenji Ishii,[b] Kunihiro Chihara,[a] and Kiichi Ishiwata[b]

[a]*Graduate School of Information Science, Nara Institute of Science and Technology, Japan*
[b]*Positron Medical Center, Tokyo Metropolitan Institute of Gerontology, 1-1, Naka, Itabashi, Tokyo 173-0022, Japan*
[c]*Japan Society for the Promotion of Science, Japan*

Received 31 July 2006; revised 20 October 2006; accepted 27 November 2006
Available online 19 January 2007

The objective of this study was to establish the kinetic analysis for mapping sigma$_1$ receptors (σ1Rs) in the human brain by positron emission tomography (PET) with [^{11}C]SA4503. The σ1Rs are considered to be involved in various neurological and psychiatric diseases. [^{11}C]SA4503 is a recently developed radioligand with high and selective affinity for σ1Rs, and we have first applied it to clinical studies. Nine healthy male subjects each underwent a dynamic 90-min PET scan after injection of [^{11}C]SA4503. In addition to the baseline measurement, three of the nine subjects underwent a second [^{11}C] SA4503-PET after partial blockade of σ1Rs by oral administration of haloperidol, a sigma receptor antagonist. Full kinetic analysis using two times nonlinear estimations was applied for fitting a two-tissue three-compartment model to determine the binding potential (BP) and total distribution volume (tDV) of [^{11}C]SA4503. Graphical analysis with a Logan plot was also applied for estimations of tDV. The regional distribution patterns of BP and tDV in 11 regions were compatible with those of previously reported σ1Rs *in vitro*. The reduced binding sites of σ1Rs by haloperidol were appropriately evaluated. The tDVs derived from the two methods matched each other well. The Logan plot offered images of the tDV, which reflected σ1R densities, and the tDV in the images decreased after haloperidol loading. Moreover, comparison of BPs calculated with and without metabolite correction for plasma input function indicated that the metabolite correction could be omitted. We concluded that this method enables the quantitative analysis of σ1Rs in the human brain.
© 2006 Elsevier Inc. All rights reserved.

Introduction

Sigma receptors are classified into sigma$_1$ and sigma$_2$ subtypes. The former was cloned but the latter was not. These subtypes display a different tissue distribution and a distinct physiological and pharmacological profile in the central and peripheral nervous system. The receptors are related to neurological and psychiatric neurophysiologies (Su, 1993; Su and Hayashi, 2003; Junien and Leonard, 1989). In the central nervous system (CNS), the sigma$_1$ receptors (σ1Rs) might play a role as a modulator of signal transduction in neurotransmitter systems such as *N*-methyl-D-aspartate (NMDA) receptors. Peripherally, the two sigma receptor subtypes are also expressed on tumor cells, where they could be of prognostic relevance. The discovery of new specific sigma receptor ligands demonstrated that sigma receptors are novel targets for the therapeutic treatment of neuropsychiatric diseases (schizophrenia, depression, and cognition) and brain ischemia and also for treating cancer (Hashimoto and Ishiwata, 2006). In several studies on postmortem brains taken from individuals with schizophrenia and Alzheimer's disease, these brains have altered densities of σ1Rs (Weissman et al., 1991; Shibuya et al., 1992; Jansen et al., 1993; Helmeste et al., 1996). Thus, the sigma receptors in the CNS are an interesting target for molecular imaging with positron emission tomography (PET) and single photon emission computed tomography (SPECT). These imaging techniques targeting sigma receptors have also provided the opportunity for the development of new drugs, evaluation of the therapeutic effects of the drugs, and better informed decisions about appropriate dosage of drugs in relation to neurological and psychiatric disorders. So far, many radioligands have been proposed for the *in vivo* imaging of sigma receptors in the brain. Preliminary clinical application of the two PET candidates, 1-(3,4-dimethoxyphenthyl)-4-(3-phenylpropyl)-piperazine hydrochloride ([^{11}C]SA4503; Fig. 1) and 1-(3-[^{18}F] fluoropropyl)-4-(4-cyanophenoxymethyl)piperidine ([^{18}F]FPS), and the clinical application of tumor imaging by SPECT were reviewed (Hashimoto and Ishiwata, 2006). Recently, [^{11}C]SA4503-PET was applied to patients with Parkinson's disease (Mishina et al., 2005). More recently, Mach et al. (2005) visualized σ1Rs in monkey brains by PET with *N*-[^{18}F]4′-fluorobenzylpiperidin-4yl-(2-fluorophenyl) acetamide ([^{18}F]FBFPA) (2005), and Stone et al. (2006) succeeded the mapping σ1Rs in the human brain by SPECT

* Corresponding author. Fax: +81 3 3964 2188.
E-mail address: ukimura@ieee.org (Y. Kimura).
Available online on ScienceDirect (www.sciencedirect.com).

1053-8119/$ - see front matter © 2006 Elsevier Inc. All rights reserved.
doi:10.1016/j.neuroimage.2006.11.055

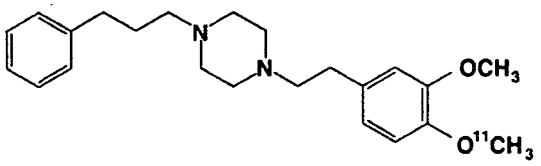

Fig. 1. Chemical structure of [^{11}C]SA4503.

with 1-(*trans*-[^{123}I]iodopropen-2-yl)-4-[(4-cyanophenoxy)methyl] piperidine ([^{123}I]TPCNE).

SA4503 has been originally developed by Matsuno and co-workers and has high affinity (IC_{50}, 17.4 nM) and high selectivity ($sigma_1/sigma_2$, 103) for σ1Rs but low affinity for other receptors such as dopamine D_2 and histamine H_1 receptors (Matsuno et al., 1996; Matsuno and Mita, 1998). Kawamura et al. (2000a, b) demonstrated that the carbon-11 labeled SA4503 selectively bound *in vivo* to σ1Rs, but not to $sigma_2$ and other receptors. Further *in vivo* studies on rodents (Ishiwata et al., 2003), cats (Kawamura et al., 2000a) and monkeys (Ishiwata et al., 2001; Kawamura et al., 2003) have demonstrated that [^{11}C]SA4503-PET has the potential to map σ1Rs. In addition, the application of [^{11}C]SA4503-PET to patients with Parkinson's disease or Alzheimer's diseases revealed the regional alteration of σ1Rs in the brains of these subjects (Mishina et al., 2005; Hashimoto and Ishiwata, 2006).

Thus, our aim in this study was to establish a quantitative way of evaluating the binding of [^{11}C]SA4503 to σ1Rs in the human brain. We performed [^{11}C]SA4503-PET in healthy young adults. First, a method for full compartment analysis was investigated, and a baseline measurement was established. Then, the method was validated for [^{11}C]SA4503-PET under haloperidol challenge, where the available binding sites of σ1Rs in the brain were artificially changed by partial blockade using haloperidol, a typical and nonselective sigma receptor antagonist (Ishiwata et al., 2001, 2003). Furthermore, a graphical analysis using the Logan plot (Logan et al., 1990) was applied to the data to visualize a spatial distribution of the binding parameter of [^{11}C]SA4503 with σ1Rs. The Logan plot is a faster and more stable method for estimation of total distribution volume (tDV) of the PET radioligand in comparison with a compartment model analysis based on a nonlinear estimation (NLE). The possibility of omitting metabolite correction for the plasma input function was also studied to conveniently apply [^{11}C]SA4503-PET to various clinical studies.

Materials and methods

Subjects and study protocol

Nine normal male volunteers with a mean age of 28±4 years were recruited. They had no neurological disorders and no abnormalities in MRIs of their brains. All subjects underwent a PET scan with [^{11}C]SA4503 as the baseline. After a 2–6 weeks interval, three of the nine subjects were given 3 mg of haloperidol orally, and 18 h later a second [^{11}C]SA4503-PET was performed. Upon treatment with haloperidol, a nonselective sigma receptor antagonist, the σ1Rs in the brain were partially blocked (Ishiwata et al., 2001, 2003), and a reduced density of σ1Rs was apparently produced.

[^{11}C]SA4503 was prepared as previously described (Kawamura et al., 2000a,b). The injected doses (mean±standard deviation (SD)) and the specific activity were 587±177 MBq/13.2±25.7 nmol and 57±11 TBq/mmol at the baseline condition (n=9), and 435±306 MBq/18.6±11.1 nmol and 21±26 TBq/mmol at the haloperidol loading condition (n=3).

The Ethics Committee of Tokyo Metropolitan Institute of Gerontology approved the study protocol, and informed consent was given by all subjects.

PET data acquisition

The PET camera used was a SET-2400 (Shimadzu Co., Kyoto, Japan), which had an axial field-of-view of 20 cm, acquired 63 slices at a center-to-center interval of 3.125 mm and had a spatial resolution of 4.4 mm full width at half maximum (FWHM) and a *Z*-axis resolution of 6.5 mm FWHM (Fujiwara et al., 1997). The 5 min transmission data were acquired with a rotating [^{68}Ge]/[^{68}Ga] line source to correct for attenuation. Then, [^{11}C]SA4503 was injected intravenously into each subject and a 90 min dynamic scan in 2D mode (10 s×6 frames, 30 s×3 frames, 60 s×5 frames, 150 s×5 frames and 300 s×14 frames) was performed, with 27 arterial blood samplings at 10, 20, 30, 40, 50, 60, 70, 80, 90, 100, 110, 120, 135 and 150 s and 3, 5, 7.5, 10, 15, 20, 30, 40, 50, 60, 70, 80 and 90 min. Each blood volume sample was 1 mL. To analyze the labeled metabolites, 2 mL of additional blood was obtained at 3, 5, 10, 15, 20, 30, 40 and 60 min. The plasma obtained by centrifugation was weighed and the radioactivity was measured with a well-type gamma-counter (BSS-1; Shimadzu Co., Kyoto, Japan), the sensitivity of which was calibrated with the PET camera. Thus, the time activity curve in arterial plasma (pTAC) was calculated as becquerels per milliliter.

Metabolites of [^{11}C]SA4503 in the plasma sampled were analyzed by high-performance liquid chromatography (HPLC) in accordance with a previously described method (Kawamura et al., 2000b). Briefly, 0.8–0.9 mL plasma was treated with one third volume of acetonitrile containing 20% trichloroacetic acid. After centrifugation, the homogenate was divided into an acid-soluble supernatant and a precipitate. The latter was washed twice with 1.0 mL of acetonitrile containing 10% trichloroacetic acid. The supernatant was diluted with 50 mM sodium acetate (pH 4.5) until the concentration of acetonitrile was 40%. Most radioactivity (>95%) in the plasma was recovered in the acid-soluble supernatant. Then, the solution was analyzed by HPLC: column, Nova-pak C18 (8 mm×100 mm; Waters, Milford, MA); eluent, acetonitrile: 50 mM sodium acetate, pH 4.5 (4:6, v/v); flow rate, 2 mL/min; and radioactivity monitor, FLO-ONE/Beta A200 (Packard, Meriden, CT). The recovery of radioactivity in the HPLC analysis was essentially quantitative.

Metabolite correction was made to pTAC values in subsequent data analyses. For this correction, the empirical function proposed by Watabe et al. (2000), $1/(1+(\alpha t)^2)^{\beta}$, was fitted with the Nelder–Meads simplex algorithm (Nelder and Mead, 1965) using a least squares method with initial guesses of 0.1 for both α and β (Kimura et al., 2004).

The dynamic image was reconstructed with a back-projection algorithm using a Butterworth filter with a cut-off frequency of 1.25 cycles/cm. The data were collected in a 128×128×63 matrix, and the voxel size was 2×2×3.125 mm. PET images were co-registered with MRI using the Automated Medical Images Registration (AMIR) program (Ardekani et al., 1995), and the regions of interest (ROIs) were located on the frontal, temporal, parietal, and occipital cortices, hippocampus, caudate, putamen, thalamus, anterior cingulated gyrus, cerebellar vermis

and cerebellar hemisphere. The sizes of the ROIs were between 1.5 mm^3 and 36.3 mm^3 (mean±SD=11.3±8.6 mm^3). Time activity curves in the tissues (tTACs) were calculated as becquerels per milliliter.

Kinetic analysis

Based on the assumption that the nonspecific binding component is in equilibrium with a free compartment (Koeppe et al., 1991), a two-tissue three-compartment model was fitted on the tTAC. The composition and relation of the three compartments are shown in Fig. 2; C_p, C_f and C_b denote the concentration of radioligand in arterial plasma, free compartment and specifically bound compartment, respectively; K_1 and k_2 denote rate constants of delivery from plasma to brain tissue through the blood–brain barrier and a clearance from tissue to plasma; k_3 and k_4 are association and dissociation rate constants, respectively, between the free component and the specifically bound component.

The estimation process comprised two steps for stable estimations. In the first step, a delay between tTACs and pTAC was estimated with the rate parameters because it was more sensitive than other parameters. In the second step, after fixing the delay, all rate constants were estimated. Both steps were based on NLE and were implemented using the interior-reflective Newton method (Coleman and Branch, 1999). Blood volumes were fixed at 3%, and non-negative constraints for K_1, k_2, k_3 and k_4 were used. The SD derived from the tTAC of each ROI was used to realize stable estimation (Bard, 1974), and the evaluated values of each frame were weighted by 1/SD in the iterative calculations. Moreover, the first two frames of a PET scan after administration of [^{11}C]SA4503 were discarded before the estimation because of the small signal-to-noise ratios from slow injection of the tracer. Initial guesses were 0.4 for K_1, 0.2 for k_2, 0.3 for k_3 and 0.02 for k_4. In this study, the convergences of estimates were confirmed by additional estimations, i.e., the initial guesses of the estimation were set to the estimated results of the second step. Then, a distribution volume of the free compartment and a tDV were calculated as K_1/k_2 and $(K_1/k_2)(1+k_3/k_4)$, respectively, and a binding potential (BP) was computed as k_3/k_4 (Mintun et al., 1984). To investigate the possibility of omitting the metabolite correction for pTAC, BPs with and without metabolite-corrected pTACs were compared with each other.

Additionally, the Logan plot (Logan et al., 1990) was applied to the tTAC of each ROI and to the dynamic images. The time intervals, especially the starting time for the Logan plot, were examined.

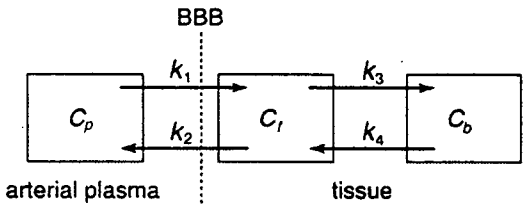

Fig. 2. Two-tissue three-compartment model. C_p is the compartment for arterial plasma, C_f is the free compartment of tissue and C_b is the specifically bound compartment of tissue. K_1 and k_2 are rate constants for the radioligand transfer between arterial plasma and brain tissue through the blood–brain barrier (BBB), and k_3 and k_4 are rate constants between free and specific binding components.

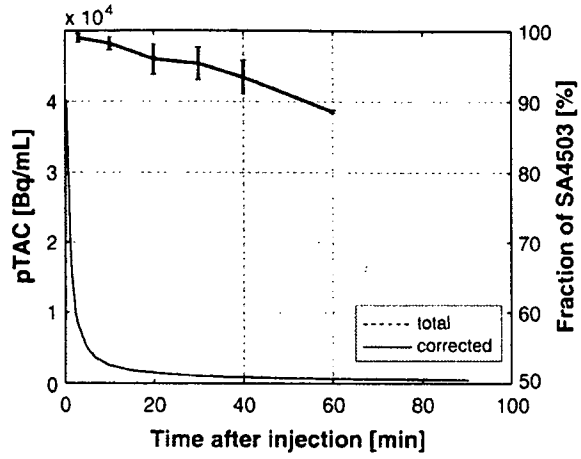

Fig. 3. Typical time–activity curve and the amount of intact [^{11}C]SA4503 in arterial plasma. Total radioactivity and metabolite corrected radioactivity are plotted in dashed and solid lines, respectively. The mean with standard deviation of the amount of intact [^{11}C]SA4503 is shown in an upper curve (n=12). At 60 min, 89% of administered [^{11}C]SA4503 remained in an intact form.

Results

pTACs and tTACs

Time courses for the fraction of unchanged [^{11}C]SA4503 in plasma and pTACs with and without metabolite correction are shown in Fig. 3. Eighty-nine percent of the administered [^{11}C]SA4503 remained in an intact form 60 min after injection. Metabolism was not altered between the baseline and haloperidol loading: their ratios of an intact form (mean±SD) were 94.7±2.2% and 97.6±0.9%, respectively, 30 min postinjection. The plots in Fig. 4 describe typical tTACs in the parietal cortex, frontal cortex

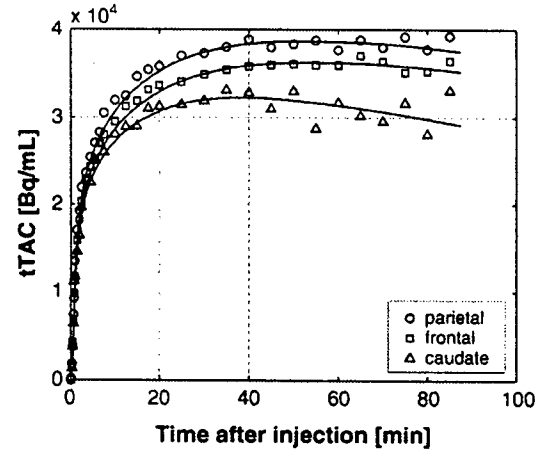

Fig. 4. Typical time–activity curves of the parietal cortex, frontal cortex and caudate in baseline conditions. The predicted curves, estimated by proposed nonlinear estimation algorithm, are superimposed on the time–activity curves.

Table 1
Estimated kinetic parameters (mean±SD, $n=9$) at baseline conditions in the brain using a nonlinear estimation algorithm

	K_1 [mL/g/min]	k_2 [1/min]	k_3 [1/min]	k_4 [1/min]	Distribution volume of free compartment [mL/g]	Total distribution volume [mL/g]	Binding potential
Frontal cortex	0.49±0.080	0.19±0.024	0.43±0.065	0.024±0.0044	2.6±0.60	49±8.0	19±4.5
Temporal cortex	0.43±0.065	0.20±0.029	0.47±0.084	0.021±0.0040	2.2±0.52	51±11.1	23±6.0
Parietal cortex	0.48±0.091	0.21±0.036	0.47±0.092	0.023±0.0047	2.4±0.61	49±7.1	21±8.4
Occipital cortex	0.53±0.085	0.20±0.004	0.41±0.056	0.023±0.0042	2.6±0.41	50±10.0	18±4.6
Hippocampus	0.43±0.074	0.25±0.094	0.46±0.113	0.018±0.0050	1.9±0.67	50±9.5	30±18.7
Caudate	0.52±0.103	0.20±0.014	0.42±0.076	0.028±0.0052	2.6±0.43	42±6.8	15±2.1
Putamen	0.56±0.105	0.20±0.025	0.44±0.068	0.027±0.0036	2.8±0.42	47±6.9	16±3.3
Thalamus	0.55±0.090	0.20±0.017	0.42±0.040	0.023±0.0035	2.8±0.32	53±8.6	19±3.4
Anterior cingulated gyrus	0.51±0.089	0.20±0.008	0.44±0.054	0.021±0.0023	2.5±0.39	56±9.6	22±4.2
Cerebellar vermis	0.50±0.052	0.20±0.009	0.49±0.063	0.020±0.0032	2.5±0.24	64±8.9	25±4.7
Cerebellar hemisphere	0.49±0.063	0.20±0.005	0.54±0.084	0.020±0.0024	2.4±0.29	70±11.4	28±5.7

and caudate in the baseline condition. The radioactivity gradually accumulated in tissues.

Kinetics

The results of curve-fitting are superimposed in Fig. 4. The time courses are described well with the compartment analysis. The estimated kinetic parameters in 11 regions of the brain using the NLE algorithm are summarized in Table 1. In the third estimation for the validation of the convergence, 94% of the estimates converged to within 10% of the results of the proposed two-step estimation, demonstrating the stability of the proposed estimation process. BPs and tDVs were significantly decreased after haloperidol loading in all regions investigated (Table 2).

Fig. 5 represents the influence of metabolite correction for pTAC on BP. Good agreement was observed between the two estimates ($y=0.87x+0.58$, $r^2=0.98$). The pTAC without metabolite correction caused an underestimation of 13% for the BPs, and no regional, subject-oriented, or pharmacological loading dependencies were found in the underestimation.

Table 2
The total distribution volumes and binding potentials (mean±SD, $n=3$) at baseline and haloperidol loading conditions in the brain tissues of three normal subjects using a nonlinear estimation algorithm

	Total distribution volume [mL/g]		Binding potential	
	Baseline	Loading	Baseline	Loading
Frontal cortex	47±7.5	15±2.3*	21±0.7	3.8±0.9*
Temporal cortex	49±12.1	16±2.6**	25±2.2	4.8±1.0*
Parietal cortex	51±6.8	15±3.0*	29±10.4	3.9±1.4
Occipital cortex	52±12.0	16±2.2**	21±3.9	4.2±1.6**
Hippocampus	47±5.1	16±2.6*	34±12.7	6.9±2.5**
Caudate	37±3.0	14±1.5*	15±1.2	3.0±0.6*
Putamen	46±7.8	16±1.4**	17±3.6	3.6±0.3**
Thalamus	53±8.2	17±1.7**	21±1.9	4.9±1.2*
Anterior cingulated gyrus	59±13.4	16±2.9**	25±2.6	4.3±1.3*
Cerebellar vermis	65±7.6	18±1.8*	27±2.8	5.6±1.4*
Cerebellar hemisphere	69±7.1	20±2.7*	29±1.3	5.5±1.2*

The total distribution volumes and binding potentials decreased significantly after haloperidol loading: *$p<0.01$ and **$p<0.05$.

Logan plot analysis

Typical Logan plots are shown in Fig. 6. Frames from 30 min to 90 min after administration were used for Logan plot analysis, and good linear relationships were observed in the plots of baseline and haloperidol loading conditions for most regions investigated. The linearity tended to worsen for small regions, such as the cerebellar vermis, and these tDVs were underestimated for the regions. Changes in the estimated tDVs in accordance with the starting time of the data used for the estimations are shown in Fig. 7. The starting time affected the estimated tDVs. However, the effects were less than 10% when the starting time was changed from 20 min to 40 min.

A comparison between the tDVs estimated by NLE and those estimated by Logan plot analysis is shown in Fig. 8. The data obtained from all regions of all scans except for those of the cerebellar vermis have been plotted. There is good coincidence

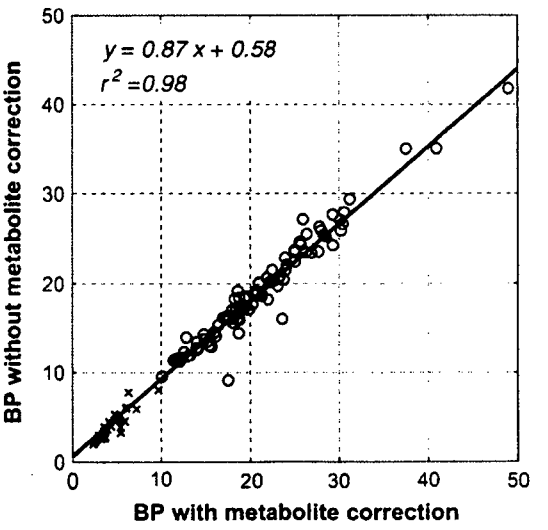

Fig. 5. Comparison of binding potentials, with and without metabolite correction, estimated by proposed full kinetic analysis. All ROIs obtained from each subject are plotted: circles represent data from the baseline condition, and crosses represent data from the haloperidol loading condition.

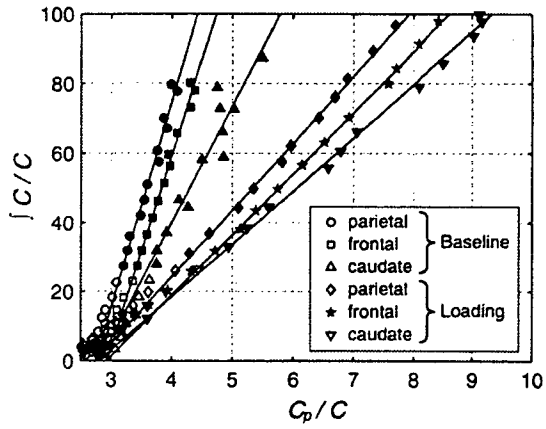

Fig. 6. Typical Logan plots. The plots for the parietal cortex, frontal cortex and caudate in baseline and haloperidol loading conditions are presented. C and C_p denote the measured time course of radioactivity in tissues and arterial plasma, respectively. Fitted lines derived from regression analysis using the data recorded from 30 to 90 min after administration of [^{11}C] SA4503 are superimposed. Data used for the line estimation are shown as solid bullets.

between both estimates ($y=0.93x+2.36$, $r^2=0.89$). Compared with the tDVs estimated by NLE, those in the cerebellar vermis derived from Logan plot analysis were underestimated because of the noise included in the tTAC. Thus, the tDVs in the cerebellar vermis were not used in this validation of the NLE method.

Images of tDV are shown in Fig. 9. tDV values were large in the cortices and basal ganglia and small in the white matter, and they significantly decreased after haloperidol loading. tDV values in Fig. 9 were smaller than those in the NLE (Table 1).

Discussion

The σ1R is related to some diseases of the central nervous system, and [^{11}C]SA4503 is used as a probe for mapping σ1Rs in the human brain. Throughout this study, a way of kinetically analyzing of [^{11}C]SA4503 has been considered.

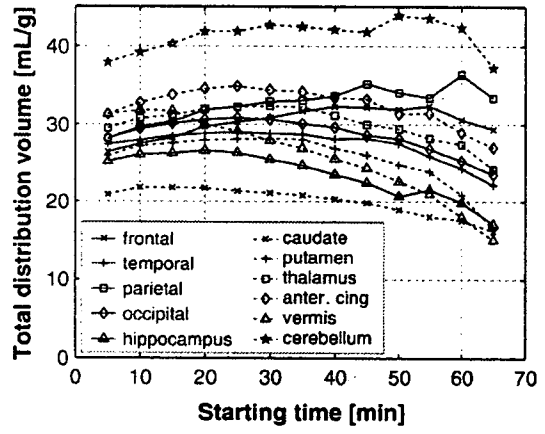

Fig. 7. Effects of starting time on the estimation of total distribution volume (tDV). A Logan plot was applied using varying starting times for the estimation. The starting time varied from 5 to 65 min, and the end time was fixed at 90 min.

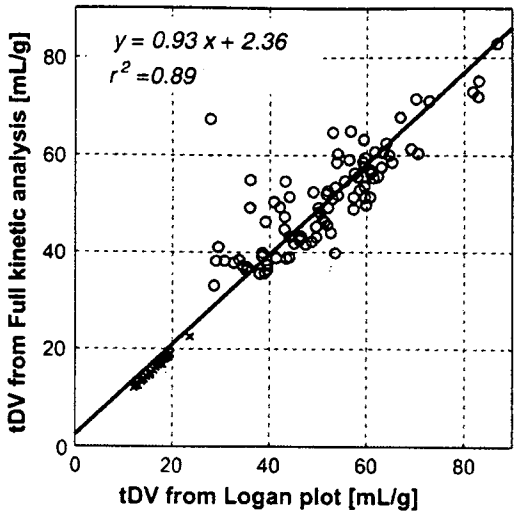

Fig. 8. Validation of the estimates of total distribution volumes. The total distribution volumes estimated by compartment model analysis (ordinate) were compared with those estimated by Logan plot analysis (abscissa). All ROIs obtained from all subjects are plotted: circles represent data from the baseline condition, and crosses represent data from the haloperidol loading condition.

First, compartmental analysis of [^{11}C]SA4503 in the brain was investigated. Theoretically, six parameters should be estimated in the two-tissue three-compartment model: K_1, k_2, k_3, k_4, delay, and blood volume. However, under an exact measurement situation, it is not feasible to estimate all the parameters simultaneously. In general, an estimation algorithm suffers from instability and dependency on the initial guess because of the noise in the tTAC. Additionally, the sensitivity of k parameters to a cost function for parameter estimation is much lower than that of blood volume or delay. Therefore, the practical implementation of the kinetic analysis means that parameters are estimated based on physiological aspects of the target neuroreceptor and the signal-to-noise ratio in the measured tTAC. Thus, reduction of the number of estimated parameters should be considered. It is physiologically reasonable to assume that blood volume is common to all brain regions, and this was fixed at 3% (Martin et al., 1987). The delay between tTAC and pTAC was also more sensitive than k parameters, and a sensitive parameter was converged on more quickly than the other parameters. In this study, five parameters (K_1, k_2, k_3, k_4, and delay) were estimated simultaneously in the first step of the estimation, then the delay estimate was used in the fixed parameters of the second step. Only four k parameters were estimated in the second step. Consequently, stable compartment model analysis could be accomplished and 94% of estimations could be considered reliable because they led to convergence within a 10% neighboring region of the estimation.

Second, the compartmental analysis was validated using the Logan plot. The Logan plot can estimate a stable tDV because it is implemented with a linear estimation, so it does not suffer from the problems of initial guess and misconvergency to a local minimum. As shown in Fig. 6, linear relationships were established in Logan plot analysis, demonstrating that the Logan plot is applicable to the analysis of [^{11}C]SA4503. As pointed out by Ichise et al. (2002), the starting time for the Logan plot affects the estimates if a tTAC showed slow kinetics. As shown in Fig. 4, the time course and

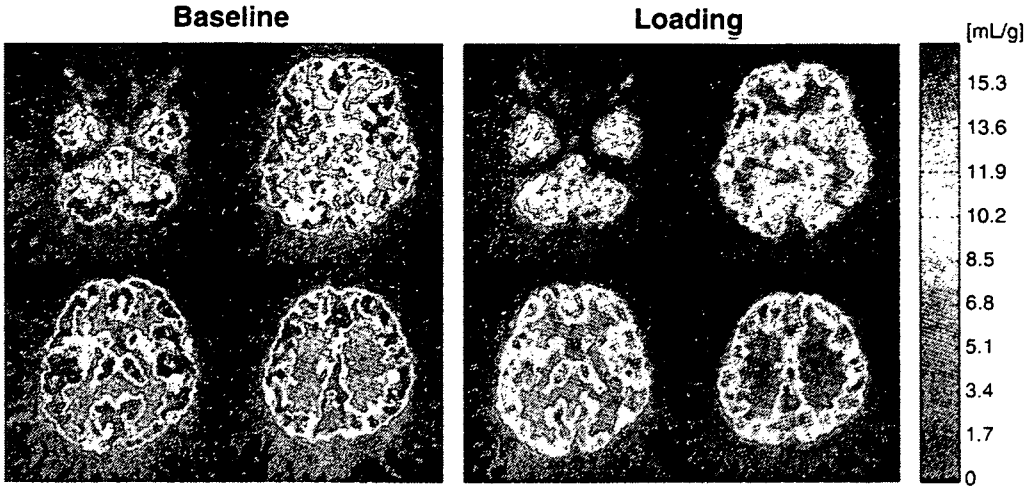

Fig. 9. Image of total distribution volumes derived with a Logan plot. The data from 30 to 90 min were applied to the Logan plot analysis.

activity of [^{11}C]SA4503 in the brain were slow and/or tended to increase after the first rapid incorporation; therefore, the starting time was sensitive to the estimated tDV. Acceptable candidates, within 20 to 40 min, were used as starting times for the Logan plot and were examined. No significant difference in estimated tDVs occurred by changing the starting time from 20 min to 40 min.

As shown in Fig. 8, the estimated tDVs from the kinetic analysis with NLE and Logan plot analysis matched each other well. The Logan plot offered stable estimates of tDV and gave more validity to our method for the kinetic analysis. The subsequent tDV images of the human brain (Fig. 9), as well as the regional distribution of the ROI-based BP (Table 1), may resemble the distribution patterns of the binding of radioligands in primate brains using an *in vitro* binding assay and autoradiography, where sigma receptors are widely distributed with different densities (Weissman et al., 1988; Shibuya et al., 1992; Mash and Zabetian, 1992). However, the radioligands used *in vitro* were not selective enough for σ1R when compared with [^{11}C]SA4503 in the present study. [^{11}C]SA4503-PET apparently exhibited the highest tDV in the cerebellum, but BP in the cerebellum was not highest (Table 1). A SPECT ligand [^{123}I] TPCNE also showed high binding in the cerebellum of humans (Stone et al., 2006); however, compared to these two radioligands, the uptake (not quantitative binding parameters) of a PET ligand [^{18}F]FBFPA in the cerebellum was relatively low in monkeys (Mach et al., 2005). In our previous study of [^{11}C] SA4503-PET using monkeys, the highest BP of [^{11}C]SA4503 was observed in the hippocampus as shown in the human brain (Table 1) followed by the cingulated cortex, frontal cortex, thalamus and cerebellar hemisphere (Kawamura et al., 2003). Taken together these findings, there may be a slight species difference between humans and non-human primates.

A haloperidol loading study also confirms the validity of our proposed method. In this study, the available binding sites of σ1Rs in the brain were considerably lowered by partial blockade with an oral administration of haloperidol (3 mg, 18 h prior the PET scan) (Ishiwata et al., 2003); however, BP and tDV were evaluated with similar accuracy, as observed in the baseline (Figs. 5, 6 and 8). These results indicate that the reduced densities of σ1Rs in brains from individuals with neurological disorders can be reliably evaluated. When we assessed the σ1R occupancy with haloperidol, when the occupancy rate was calculated to be $100\times[(\text{BP in baseline})-(\text{BP in haloperidol loading})]/(\text{BP in baseline})$, the σ1R occupancy rates were about 80% in all regions investigated: the highest occupancy was 87% in the parietal and the lowest was 77% in the thalamus. Therefore, the preliminary experiment with haloperidol loading also demonstrates that [^{11}C]SA4503-PET could be useful for evaluating the therapeutic effects of the drugs and for the development of new drugs in term of the measurement of σ1R occupancy rates. It should be noted that haloperidol is a nonselective antagonist for sigma receptors and also binds other receptors such as dopamine D_2-like receptors. Therefore, the present study does not demonstrate the σ1R-selective binding of [^{11}C]SA4503. However, the use of haloperidol as a blocker is interesting because it is clinically used (usually 3–10 mg) as a typical antipsychotic drug. We previously reported that the σ1R blockade by haloperidol in the mouse brain continued slightly longer than the dopamine D_2-like receptor blockade (Ishiwata et al., 2003). Recently, we confirmed that the receptor occupancy rate for σ1R (approximately 80%) in the human brain was higher than that for dopamine D_2-like receptor (approximately 60%) after the oral administration of haloperidol (3 mg) in a similar experimental protocol (Ishiwata et al., 2006). Concerning the haloperidol challenge, Stone et al. (2006) also demonstrated that an oral administration of haloperidol (2.5 mg, approximately 1 h before the SPECT scan) greatly decreased the binding of [^{123}I]TPCNE to σ1Rs with a different extent in the brain regions: from 42% reduction in the cerebellum to 73% reduction in the thalamus ($n=1$). The blockade for σ1Rs by [^{123}I]TPCNE seems slightly smaller than that by [^{11}C]SA4503. A main reason for the difference may be the period between haloperidol administration and imaging, i.e., a 1-h interval may be early for an oral administration. The other reason may be due to selectivity of the two radioligands. The $sigma_1/sigma_2$ selectivity for [^{11}C]SA4503 was 106 (Matsuno et al., 1996), while that for [^{123}I]TPCNE was 58 (Waterhouse et al., 1997). The affinity of [^{11}C]SA4503 for $sigma_2$ receptor ($IC_{50}=1784$ nM) was much lower than that of [^{123}I]TPCNE (Ki=38.8 nM) (Waterhouse et al., 1997).

In Logan plot analysis, the noise of tTAC causes an underestimation of tDV (Slifstein and Laruelle, 2000). In ROI-based analysis, the mean of the dynamic image was used because it

reduced the noises. However, because the noise remained high in the tTACs for small regions of the brain, it caused an underestimation of tDV in the cerebellar vermis, which was the smallest region. Additionally, the tDV of the parametric images, which were affected by the noise of the tTACs, were estimated to be smaller than the estimates for the ROIs. Nevertheless, Logan plot analysis easily provides images of tDV. As shown in Table 1, the distribution volume of the ligand in the free component was much smaller than the tDV, which demonstrates that the specific binding of [^{11}C]SA4503 reached about 95% of tDVs in all brain regions investigated. Therefore, tDV images essentially reflect the density of σ1Rs. Thus, Fig. 9 indicates that σ1Rs are widely spread with different densities in the whole brain and that a significant decrement of tDVs occurred by blockade with haloperidol.

Let us consider the requirement of metabolite correction for pTAC. Metabolite correction is usually required for kinetic analysis to compensate for the radioligand that is metabolized peripherally. As shown in Fig. 3, the intact form of [^{11}C]SA4503 makes up about 90% of the radioactivity in arterial plasma over 60 min, suggesting that a slow peripheral metabolism of [^{11}C]SA4503 occurs. Moreover, from a practical point of view, precise measurement of small amounts of labeled metabolites is difficult, especially over time, because of the very rapid clearance of [^{11}C] SA4503 from plasma. Therefore, the omission of metabolite correction is appropriate. The BP values without metabolite correction were 13% lower than those with metabolite correction; however, BP values with and without metabolite correction showed an almost identical relationship in all subjects, all ROIs and the two conditions: baseline and haloperidol loading. Therefore, metabolite correction can be reasonably avoided. It should be noted that [^{11}C]SA4503 was metabolically more stable in humans than in rats (the intact form in plasma, approximately 95% versus 80%, respectively, of 30 min postinjection), and the haloperidol challenge did not alter the metabolism. Stability of [^{11}C]SA4503 in plasma may be explained by the fact that the tracer mainly underwent biliary excretion (Kawamura et al., 2000b; van Waarde et al., 2004), which might result in scarce recirculation of labeled metabolites into the plasma.

Conclusion

We conclude that our proposed method using a two-tissue three-compartment model is appropriate to provide BP and tDV for the kinetic analysis of [^{11}C]SA4503-PET in human brain tissue. The tDV derived matched well with that derived from the Logan plot analysis, whose images enable visualization of the spatial distribution of σ1Rs. The reduced binding sites of σ1Rs by haloperidol challenge were appropriately evaluated. Moreover, comparison of BPs calculated with and without metabolite correction for the plasma input function indicated that the metabolite correction could be omitted. We concluded that this method enables the quantitative analysis of σ1Rs in the human brain.

Acknowledgments

This work is supported in part by the Grant-in-Aid for the 21st Century COE from the Ministry of Education, Culture, Sports, Science and Technology of Japan, by the Japan Society for the Promotion of Science, the Grant-in-Aid for JSPS Research Fellows, No. 18-6919 in 2006–2008 and by the Grant-in-Aid for Scientific Research by the Japan Society for the Promotion of Science by Scientific Research No. 18591373 in 2006–2007.

References

Ardekani, B.A., Braun, M., Hutton, B.F., Kanno, I., Iida, H., 1995. A fully automatic multimodality image registration algorithm. J. Comput. Assist. Tomogr. 19, 615–623.

Bard, Y., 1974. Weighted least squares. Nonlinear Parameter Estimation. Academic Press, New York, pp. 56–57. Chap. 4-3.

Coleman, T., Branch, M.A., 1999. Optimization Toolbox User's Guide. MathWorks Inc., Natick, MA.

Fujiwara, T., Watanuki, S., Yamamoto, S., Miyake, M., Seo, S., Itoh, M., Ishii, K., Orihara, H., Fukuda, H., Satoh, T., Kitamura, K., Tanaka, K., Takahashi, S., 1997. Performance evaluation of a large axial field-of-view PET scanner: SET-2400W. Ann. Nucl. Med. 11, 307–313.

Hashimoto, K., Ishiwata, K., 2006. Sigma receptor ligands: possible application as therapeutic drugs and as radiopharmaceuticals. Curr. Pharm. Des. 12, 3915–3928.

Helmeste, D.M., Tang, S.W., Bunney Jr., W.E., Potkin, S.G., Jones, E.G., 1996. Decrease in sigma but no increase in striatal dopamine D4 sites in schizophrenic brains. Eur. J. Pharmacol. 314 (3), R3–R5.

Ichise, M., Toyama, H., Innis, R.B., Carson, R.E., 2002. Strategies to improve neuroreceptor parameter estimation by linear regression analysis. J. Cereb. Blood Flow Metab. 22, 1271–1281.

Ishiwata, K., Tsukada, H., Kawamura, K., Kimura, Y., Nishiyama, S., Kobayashi, T., Matsuno, K., Senda, M., 2001. Mapping of CNS sigma$_1$ receptors in the conscious monkey: preliminary PET study with [^{11}C] SA4503. Synapse 40, 235–237.

Ishiwata, K., Kawamura, K., Kobayashi, T., Matsuno, K., 2003. Sigma$_1$ and dopamine D_2 receptors occupancy in the mouse brain after a single administration of haloperidol and two dopamine D_2-like receptor ligands. Nucl. Med. Biol. 30, 429–434.

Ishiwata, K., Oda, K., Sakata, M., Kimura, Y., Kawamura, K., Oda, K., Sasaki, T., Naganawa, M., Chihara, K., Okubo, Y., Ishii, K., 2006. A feasibility study of [^{11}C]SA4503-PET for evaluating sigma$_1$ receptor occupancy by neuroleptics: the binding of haloperidol to sigma$_1$ and dopamine D_2-like receptors. Ann. Nucl. Med. 20, 569–573.

Jansen, K.L., Faull, R.L., Storey, P., Leslie, R.A., 1993. Loss of sigma binding sites in the CA1 area of the anterior hippocampus in Alzheimer's disease correlates with CA1 pyramidal cell loss. Brain Res. 623, 299–302.

Junien, J.L., Leonard, B.E., 1989. Drugs acting on sigma and phencyclidine receptors: a review of their nature, function and possible therapeutic importance. Clin. Neuropharmacol. 12, 353–374.

Kawamura, K., Ishiwata, K., Shimada, Y., Kimura, Y., Kobayashi, T., Matsuno, K., Homma, Y., Senda, M., 2000a. Preclinical evaluation of [^{11}C]SA4503: radiation dosimetry, *in vivo* selectivity and PET imaging of sigma$_1$ receptors in the cat brain. Ann. Nucl. Med. 14, 285–292.

Kawamura, K., Ishiwata, K., Tajima, H., Ishii, S., Matsuno, K., Homma, Y., Senda, M., 2000b. *In vivo* evaluation of [^{11}C]SA4503 as a PET ligand for mapping CNS sigma$_1$ receptors. Nucl. Med. Biol. 27, 255–261.

Kawamura, K., Kimura, Y., Tsukada, H., Kobayashi, T., Nishiyama, S., Kakiuchi, T., Ohba, H., Harada, N., Matsuno, K., Ishii, K., Ishiwata, K., 2003. An increase of sigma$_1$ receptors in the aged monkey brain. Neurobiol. Aging 24, 745–752.

Kimura, Y., Ishii, K., Fukumitsu, N., Oda, K., Sasaki, T., Kawamura, K., Ishiwata, K., 2004. Quantitative analysis of adenosine A_1 receptors in human brain using positron emission tomography and [1-methyl-^{11}C]8-dicyclopropylmethyl-1-methyl-3-propylxanthine. Nucl. Med. Biol. 31, 975–981.

Koeppe, R.A., Holthoff, V.A., Frey, K.A., Kilbourn, M.R., Kuhl, D.E., 1991. Compartmental analysis of [^{11}C]flumazenil kinetics for the estimation of ligand transport rate and receptor distribution using positron emission tomography. J. Cereb. Blood Flow Metab. 11, 735–744.

Logan, J., Fower, J.S., Volkow, N.D., Wolf, A.P., Dewey, S.L., Schlyer, D.J., MacGregor, R.R., Hitzemann, R., Bendriem, B., Gatley, S.J., Christman, D.R., 1990. Graphical analysis of reversible radioligand binding from time–activity measurements applied to [*N*-^{11}C-methyl]-(−)-cocaine PET studies in human subjects. J. Cereb. Blood Flow Metab. 10, 740–747.

Mach, R.H., Gage, H.D., Buchheimer, N., Huang, Y., Kuhner, R., Wu, L., Morton, T.E., Ehrenkaufer, R.L., 2005. *N*-[^{18}F]4′-fluorobenzylpiperidin-4yl-(2-fluorophenyl) acetamide ([^{18}F]FBFPA): a potential fluorine-18 labeled PET radiotracer for imaging sigma-1 receptors in the CNS. Synapse 58, 267–274.

Martin, W.R.W., Powers, W.J., Raichle, M.E., 1987. Cerebral blood volume measured with Inhaled C^{15}O and positron emission tomography. J. Cereb. Blood Flow Metab. 7, 421–426.

Mash, D.C., Zabetian, C.P., 1992. Sigma receptors are associated with cortical limbic areas in the primate brain. Synapse 12, 195–205.

Matsuno, K., Mita, S., 1998. SA4503: a novel sigma$_1$ receptor agonist. CNS Drug Rev. 4, 1–24.

Matsuno, K., Nakazawa, M., Okamoto, K., Kawashima, Y., Mita, S., 1996. Binding properties of SA4503, a novel and selective σ_1 receptor agonist. Eur. J. Pharmacol. 306, 271–279.

Mintun, M.A., Raichle, M.E., Kilbourn, M.R., Wooten, G.F., Welch, M.J., 1984. A quantitative model for the *in vivo* assessment of drug binding sites with positron emission tomography. Ann. Neurol. 15, 217–227.

Mishina, M., Ishiwata, K., Ishii, K., Kitamura, S., Kimura, Y., Kawamura, K., Oda, K., Sasaki, T., Sakayori, O., Hamamoto, M., Kobayashi, S., Katayama, Y., 2005. Function of sigma$_1$ receptors in Parkinson's disease. Acta Neurol. Scand. 112, 103–107.

Nelder, J., Mead, R., 1965. A simplex method for function minimization. Comput. J. 7, 308–313.

Shibuya, H., Mori, H., Toru, M., 1992. Sigma receptors in schizophrenic cerebral cortices. Neurochem. Res. 17, 983–990.

Slifstein, M., Laruelle, M., 2000. Effects of statistical noise on graphic analysis of PET neuroreceptor studies. J. Nucl. Med. 41, 2083–2088.

Stone, J.M., Arstad, E., Erlandsson, K., Waterhouse, R.N., Ell, P.J., Pilowsky, L.S., 2006. [^{123}I]TPCNE-a novel SPET tracer for the sigma-1 receptor: first human studies and *in vivo* haloperidol challenge. Synapse 60, 109–117.

Su, T.P., 1993. Delineating biochemical and functional properties of sigma receptors: emerging concepts. Crit. Rev. Neurobiol. 7, 187–203.

Su, T.P., Hayashi, T., 2003. Understanding the molecular mechanism of sigma-1 receptors: towards a hypothesis that sigma-1 receptors are intracellular amplifiers for signal transduction. Curr. Med. Chem. 10, 2073–2080.

van Waarde, A., Buursma, A.R., Hospers, G.A.P., Kawamura, K., Kobayashi, T., Ishii, K., Oda, K., Ishiwata, K., Vaalburg, W., Elsinga, P.H., 2004. Tumor imaging with 2 σ-receptor ligands, [^{18}F]FE-SA5845 and [^{11}C]SA4503: a feasibility study. J. Nucl. Med. 45, 1939–1946.

Watabe, H., Channing, M.A., Der, M.G., Adams, H.R., Jagoda, E., Herscovitch, P., Eckelman, W.C., Carson, R.E., 2000. Kinetic analysis of the 5-HT$_{2A}$ ligand [^{11}C]MDL 100,907. J. Cereb. Blood Flow Metab. 20, 899–909.

Waterhouse, R.N., Mardon, K., Giles, K.M., Collier, T.L., O'Brien, J.C., 1997. Halogenated 4-(phenoxymethyl)piperidines as potential radiolabeled probes for sigma-1 receptors: *in vivo* evaluation of [^{123}I]-1-(iodopropen-2-yl)-4-[(4-cyanophenoxy)methyl]piperidine. J. Med. Chem. 40, 1657–1667.

Weissman, A.D., Su, T.P., Hedreen, J.C., London, E.D., 1988. Sigma receptors in post-mortem human brains. J. Pharmacol. Exp. Ther. 247, 29–33.

Weissman, A.D., Casanova, M.F., Kleinman, J.E., London, E.D., De Souza, E.B., 1991. Selective loss of cerebral cortical sigma, but not PCP binding sites in schizophrenia. Biol. Psychiatry 29, 41–54.

BRAIN RESEARCH 1142 (2007) 19–27

available at www.sciencedirect.com

ScienceDirect

www.elsevier.com/locate/brainres

BRAIN RESEARCH

Research Report

A comparative study of bioradiography in human brain slices and preoperative PET imaging

Toru Sasaki[a,b,*], *Tadashi Nariai*[c], *Taketoshi Maehara*[c], *Katsushige Sato*[d], *Keiich Oda*[b], *Kenji Ishii*[b]

[a]*Research Team for Molecular Biomarker, Tokyo Metropolitan Institute of Gerontology, Itabashi-ku, Tokyo 173-0015, Japan*
[b]*Positorn Medical Center, Tokyo Metropolitan Institute of Gerontology, Itabashi-ku, Tokyo 173-0015, Japan*
[c]*Department of Neurosurgery, Tokyo Medical and Dental University, Bunkyo-ku, Tokyo 113-8519, Japan*
[d]*Department of Physiology, Tokyo Medical and Dental University, Bunkyo-ku, Tokyo 113-8519, Japan*

ARTICLE INFO

Article history:
Accepted 9 January 2007
Available online 18 January 2007

Keywords:
Bioradiography
Positron emission tomography (PET)
Epilepsy
Brain slice

ABSTRACT

Novel autoradiography (bioradiography) images in human neocortical brain slices which were obtained at operation from seven patients with intractable epilepsy who had received a 2-[^{18}F]fluoro-2-deoxy-D-glucose-positron emission tomography (FDG-PET) examination preoperatively, were acquired in Krebs–Ringer medium (control condition) and that with high K^+ (high K^+ condition) containing FDG and compared with FDG-PET uptake. The FDG uptake images in rat brain slices were also acquired as a reference and compared with that in humans. In the slices incubated under high K^+, FDG uptake in both human and rat gray matter was significantly enhanced, whereas that in the white matter was not. But the variance of uptake was larger in humans than the rats. This might indicate the different degree of progress of epilepsy in the sampled brain tissues. The uptake rates of FDG in human gray matter under the control condition showed an inverse correlation with those seen in PET, which were evaluated as sampled and contralateral gyri (SG/CG) and sampled gyri and cerebellar cortex (SG/CB) ratio. On the contrary, it showed a weak positive correlation with PET under the high K^+ condition. The uptake rates of FDG in human gray matter expressed as a high K^+/control ratio, closely matched that observed by FDG-PET, which were evaluated as the SG/CG ratio and the SG/CB ratio. Our experimental system provides useful information for the interpretation of PET data in epileptics and the theoretical basis to interpret the results of metabolic studies using living human brain tissues for further use in pharmacological manipulation.

© 2007 Elsevier B.V. All rights reserved.

Introduction

Bioradiography is a novel autoradiographic method to estimate metabolism and physiological function in living tissues using positron emitter-labeled compounds for positron emission tomography (PET) (Matsumura et al., 1995; Murata et al., 1996; Sasaki et al., 2002a,b). It offers the following advantages: (1) dynamic changes in metabolic activity can be followed in living tissue, (2) environmental conditions of tissue slices can be easily controlled as required, and (3) radioligand delivery to

* *Corresponding author.* Present address: Research Team for Molecular Biomarker, Tokyo Metropolitan Institute of Gerontology, Itabashi-ku, Tokyo 173-0015, Japan.
E-mail address: tsasaki@center.tmig.or.jp (T. Sasaki).

0006-8993/$ – see front matter © 2007 Elsevier B.V. All rights reserved.
doi:10.1016/j.brainres.2007.01.036